Composition of Titan's lower atmosphere and simple surface volatiles as measured by the Cassini-Huygens probe gas chromatograph mass spectrometer experiment

H. B. Niemann,[1] S. K. Atreya,[2] J. E. Demick,[3] D. Gautier,[4] J. A. Haberman,[1] D. N. Harpold,[1] W. T. Kasprzak,[1] J. I. Lunine,[5] T. C. Owen,[6] and F. Raulin[7]

Received 25 May 2010; revised 20 August 2010; accepted 8 September 2010; published 10 December 2010.

[1] The Cassini-Huygens probe gas chromatograph mass spectrometer (GCMS) determined the composition of the Titan atmosphere from ~140 km altitude to the surface. After landing, it returned composition data of gases evaporated from the surface. Height profiles of molecular nitrogen (N_2), methane (CH_4), and molecular hydrogen (H_2) were determined. Traces were detected on the surface of evaporating methane, ethane (C_2H_6), acetylene (C_2H_2), cyanogen (C_2N_2), and carbon dioxide (CO_2). The methane data showed evidence that methane precipitation occurred recently. The methane mole fraction was $(1.48 \pm 0.09) \times 10^{-2}$ in the lower stratosphere (139.8–75.5 km) and $(5.65 \pm 0.18) \times 10^{-2}$ near the surface (6.7 km to the surface). The molecular hydrogen mole fraction was $(1.01 \pm 0.16) \times 10^{-3}$ in the atmosphere and $(9.90 \pm 0.17) \times 10^{-4}$ on the surface. Isotope ratios were 167.7 ± 0.6 for $^{14}N/^{15}N$ in molecular nitrogen, 91.1 ± 1.4 for $^{12}C/^{13}C$ in methane, and $(1.35 \pm 0.30) \times 10^{-4}$ for D/H in molecular hydrogen. The mole fractions of ^{36}Ar and radiogenic ^{40}Ar are $(2.1 \pm 0.8) \times 10^{-7}$ and $(3.39 \pm 0.12) \times 10^{-5}$, respectively. ^{22}Ne has been tentatively identified at a mole fraction of $(2.8 \pm 2.1) \times 10^{-7}$. Krypton and xenon were below the detection threshold of 1×10^{-8} mole fraction. Science data were not retrieved from the gas chromatograph subsystem as the abundance of the organic trace gases in the atmosphere and on the ground did not reach the detection threshold. Results previously published from the GCMS experiment are superseded by this publication.

Citation: Niemann, H. B., S. K. Atreya, J. E. Demick, D. Gautier, J. A. Haberman, D. N. Harpold, W. T. Kasprzak, J. I. Lunine, T. C. Owen, and F. Raulin (2010), Composition of Titan's lower atmosphere and simple surface volatiles as measured by the Cassini-Huygens probe gas chromatograph mass spectrometer experiment, *J. Geophys. Res.*, *115*, E12006, doi:10.1029/2010JE003659.

1. Introduction

[2] The gas chromatograph mass spectrometer (GCMS) instrument [*Niemann et al.*, 2002] was designed to measure the composition of the ambient atmosphere of Titan during the descent of the Huygens probe. Atmospheric data were received for 148 min beginning at an altitude of 146 km down to the surface. Although not designed to survive surface impact, the probe and the instruments did survive the impact undamaged and returned gas composition data for another 72 min until contact was lost with the Cassini orbiter [*Lebreton et al.*, 2005]. Preliminary results presented in *Niemann et al.* [2005] have been refined based on further laboratory calibration of the spare flight unit sensor and more detailed analysis of the flight data.

[3] Voyager remote sensing instruments had already identified the major and several minor constituents above Titan's tropopause [*Kunde et al.*, 1981; *Hanel et al.*, 1981; *Coustenis et al.*, 1989; *Coustenis et al.*, 1991]. These measurements were made in the stratosphere. Height profiles, isotope ratios, and noble gas concentrations were not retrieved from these data. Thus, the fate of the photochemically produced trace gases in the upper atmosphere remained obscure. Several of the Cassini orbiter instruments, e.g., the ion and neutral mass spectrometer (INMS), the composite infrared spectrometer (CIRS), and the ultraviolet imaging spectrometer (UVIS), have provided a wealth of information on the composition of organic trace gases in the stratosphere and the upper atmosphere and ionosphere, i.e., in the regions where they were first formed [*Waite et al.*,

[1]National Aeronautics and Space Administration, Greenbelt, Maryland, USA.
[2]Department of Atmospheric, Oceanic and Space Sciences, University of Michigan, Ann Arbor, Michigan, USA.
[3]Department of Physics and Physical Science, Huntington College, Montgomery, Alabama, USA.
[4]LESIA, Observatoire de Paris-Meudon, Meudon, France.
[5]Department of Physics, University of Rome Tor Vergata, Rome, Italy.
[6]Institute for Astronomy, University of Hawaii, Honolulu, Hawaii, USA.
[7]LISA, CNRS/Université Paris 12/Université Paris 7, Creteil, France.

0148-0227/10/2010JE003659

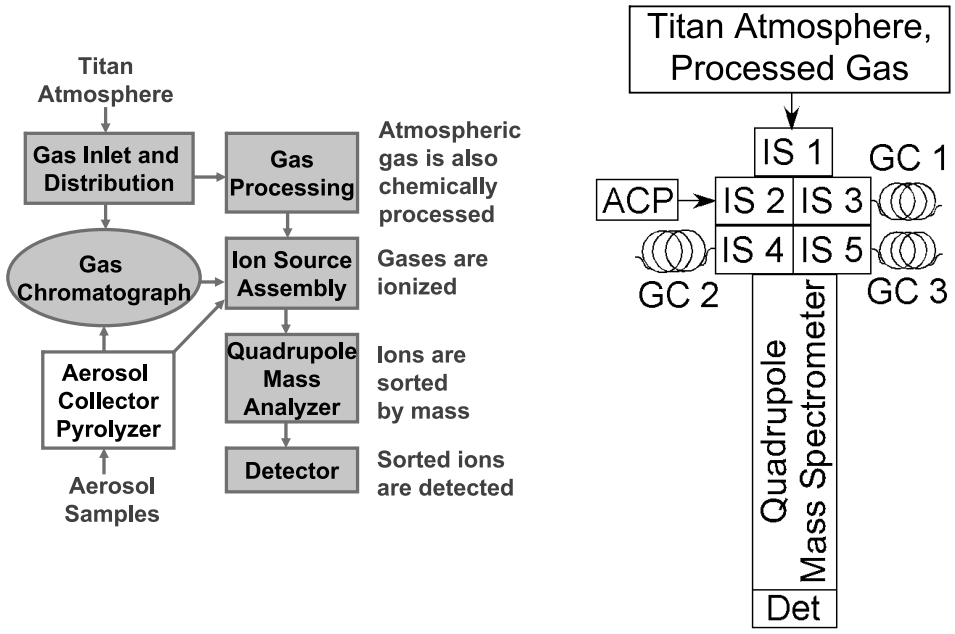

Figure 1. Schematic of the Huygens GCMS gas sampling and mass spectrometer assembly. (left) The subsystems and their interfaces and functions. (right) The multi-ion source mass spectrometer subsystem. IS1–IS5 are the ion sources. GC1–GC3 are the gas chromatograph channels.

2005, 2007; *Cui et al.*, 2009; *Magee et al.*, 2009; *Flasar et al.*, 2005; *Coustenis et al.*, 2007; *Shemansky et al.*, 2005].

[4] One of the objectives of the Huygens probe experiments was to determine the extent to which the simpler trace gases can form complex molecules, condensates, or aerosol particles that ultimately precipitate onto the surface. N_2, CH_4, H_2, and ^{40}Ar were measured in situ in the lower atmosphere by the GCMS and altitude profiles were obtained. ^{22}Ne and ^{36}Ar were detected in a batch sample in a noble gas enrichment cell. Kr and Xe were below the detection limit of the instrument for those species, and their abundances are estimated to be less than 1×10^{-8} mole fraction.

[5] Isotope ratios were determined for hydrogen from H_2 and HD, for nitrogen from $^{14}N^{14}N$ and $^{14}N^{15}N$, and for carbon from $^{12}CH_4$ and $^{13}CH_4$. These GCMS measurements provide important constraints on models for the formation of Titan and its atmosphere.

[6] After landing CH_4, C_2H_6, C_2H_2, C_2N_2, and CO_2 were detected as they evaporated from the surface directly below the probe. Benzene (C_6H_6) may also have been evaporating, but its abundance was too low to be separated unambiguously from the permanent C_6H_6 background in the instrument.

[7] The GCMS was also used to analyze the aerosol pyrolysis products from the Cassini-Huygens aerosol collector pyrolyser (ACP) experiment [*Israel et al.*, 2002]. Results obtained from that experiment were reported and discussed separately [*Israel et al.*, 2005; *Biemann*, 2006; *Israel et al.*, 2006].

[8] Identification of organic trace constituents with the three-column gas chromatograph subsystem (GC) was not possible because concentrations in the atmosphere were too low to reach the GCMS detection threshold.

[9] At the altitude of 74 km, when the probe passed through a region of extensive turbulence, ion source number 5 failed. This ion source was dedicated to obtaining data from a GC column specifically designed for the measurement of carbon monoxide (CO) since the flight mass spectrometer was not designed to separate directly N_2 and CO at $m/z = 28$.

2. Experiment Description

[10] The experiment has been described in detail by *Niemann et al.* [2002]. It was designed to measure the chemical composition of the atmosphere of Titan and to determine the isotope ratios of the major gaseous constituents. It was able to also detect gases evaporating from the surface. The GCMS analyzed gas samples from the aerosol collector pyrolyser (ACP). A detailed description of the ACP instrument is given by *Israel et al.* [2002].

2.1. Instrument

[11] A simplified block diagram of the instrument is shown in Figure 1. The instrument [*Niemann et al.*, 2002] consists of a gas inlet and distribution system, a system for pressure reduction, a gas processing system (sample enrichment and chemical scrubber cell), a three-column gas chromatograph system (GC 1, 2, 3) and a quadrupole type mass filter with a secondary electron multiplier ion detector. The interface points of the ACP with the instrument are also indicated in Figure 1 The chemical scrubber cell was used to facilitate interference free noble gas measurements, and the sample enrichment cell was intended for enriching high boiling point hydrocarbons.

[12] The mass spectrometer had five electron-impact ion sources with electron energies of 70 eV. Lower electron energy of 25 eV was used for short periodic intervals. Three

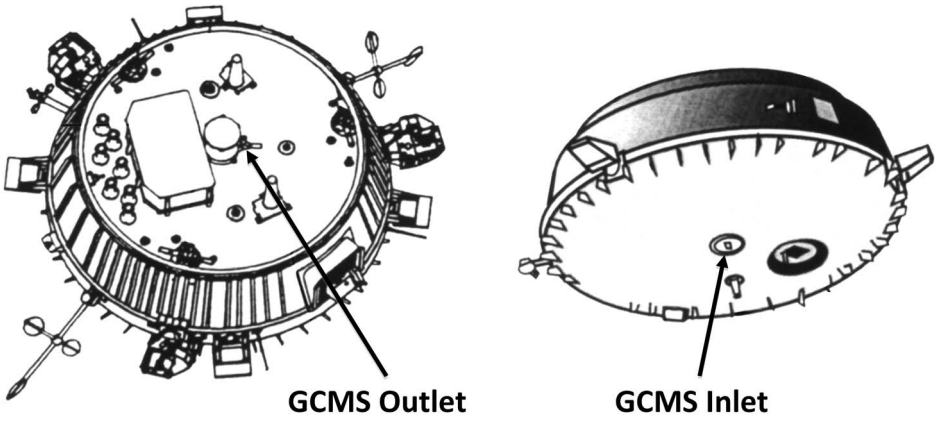

Figure 2. Illustration of the locations of the atmosphere sample inlet and outlet ports on the Huygens probe.

ion sources served as detectors for the GC columns, one was dedicated to direct atmosphere sampling, and one was for analyzing the gas samples transferred from the ACP. The multiple ion source approach allowed rapid electronic switching between sample systems and prevented cross contamination from the multiple sample sources.

[13] The gas cross talk between ion sources was less than 1×10^{-6}. The separation was achieved by pumping each ion source and the analyzer/detector regions with separate sets of chemical getters and sputter ion pumps. In addition the ion lenses of the ion sources were especially designed for low gas conductance between the ionization regions and the common mass analyzer region. The system is described in detail by *Niemann et al.* [2002].

[14] The mass filter produced flat top mass peaks that allowed rapid scanning with 5 ms per data sample. Unit step values of mass to charge ratios (m/z) from 2 to 141 were used with occasional 0.125 interval sweeps for diagnostics. The nominal detection threshold was at a mole fraction of 10^{-8}. The actual detection threshold for individual species varied depending on interference from other species and chemical noise in the ion sources. The three GC columns were selected to separate C_3 to C_8 hydrocarbons and nitriles, C_1 to C_3 hydrocarbons, and nitrogen and carbon monoxide respectively. Micron-sized capillary arrays were used to reduce the ambient pressure during the probe descent, ~3 hPa to 150 kPa, to the required ion source pressure as well as to reduce the operating pressure of the GC columns

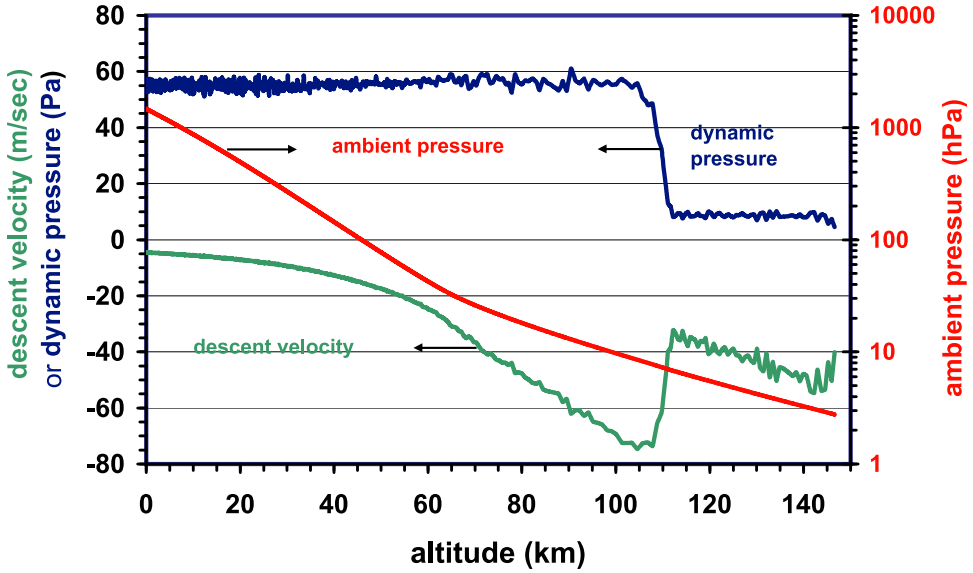

Figure 3. Ambient pressure, descent velocity, and probe dynamic pressure versus altitude during probe descent. The descent velocity and dynamic pressure share the common left-hand ordinate, while the ambient pressure uses the right-hand ordinate as indicated by the horizontal arrows next to each curve. The ambient pressure was measured by the HASI experiment. The descent velocity was determined by the DWE experiment and the Descent Trajectory Working Group (DTWG). The dynamic pressure was computed from the ambient mass density and the descent velocity.

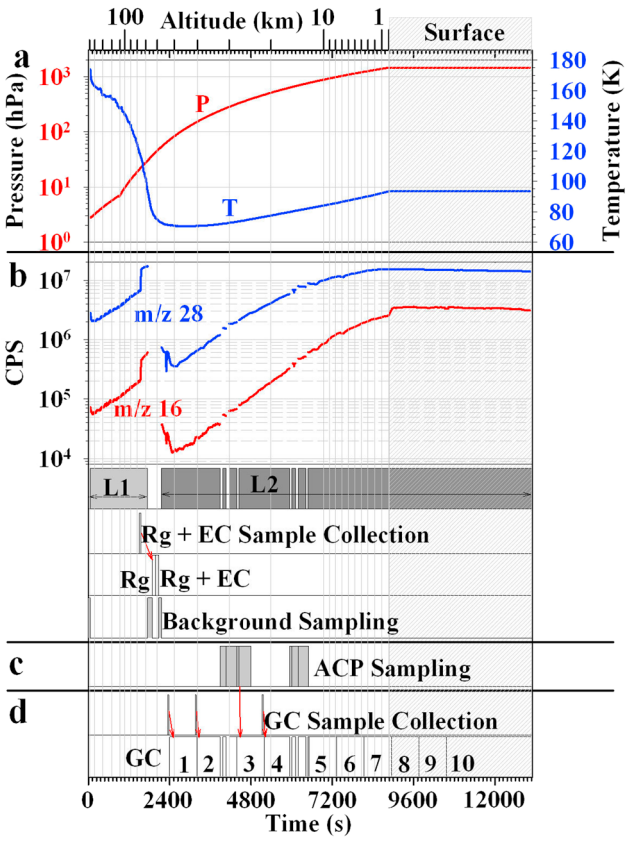

Figure 4. Ambient pressure-temperature-altitude and event profiles versus time from measurement sequence initiation. (a) Ambient pressure and temperature. (b) Raw count rates, uncorrected for pulse-pileup and/or dead-time, from ion source 1 for m/z = 28 and 16. The gaps in the m/z = 28 trace are events when the rare gas (Rg) and enrichment cell (EC) were analyzed and the ACP data were transferred and analyzed with ion source 2. (c) The time intervals when the inlet leaks L1and L2 were used are shown in the shaded areas. (d) The gas chromatograph cycles.

to 180 kPa. Two sets of capillary arrays with different gas conductance were used in sequence for the direct atmosphere ion source in order to cover the wide ambient pressure range traversed during the descent. Gases were removed from the ion sources by conductance limited getter and sputter ion pumps. The maximum ion source operating pressure was 1×10^{-4} hPa. The pressure in the mass filter was always below 1×10^{-6} hPa.

[15] The gas inlet was near the apex of the probe fairing, and the outlet was at the rear of the probe. The sample inlet and outlet locations on the probe body are shown in Figure 2. Gas flowed through a several millimeter diameter sampling tube, driven by the dynamic pressure. The dynamic pressure is the pressure differential between the stagnation pressure at the tube entrance and the ambient pressure at the tube exit. A small amount of the atmospheric gas was diverted from the flow line through the capillary leaks into the ionization region of the ion source. To minimize surface losses of trace and chemically active constituents, the capillary leaks were located so that the exit flow from the capillaries could enter the ionization region with minimal surface collisions. Upstream from the capillary leaks, the inlet line was heated to prevent condensation and to cause rapid evaporation of condensates that might flow through the sampling line. This also caused a small convective gas flow through the inlet line after landing. The gas flow through the inlet line varied with altitude during the descent from several hPa cm^3 per minute to several hundred hPa cm^3 per minute. The gas sampling system and mass spectrometer were sealed before launch and maintained under ultrahigh vacuum until jettison of the probe heat shield when the inlet and outlet seals of the sampling tube were broken and the system was exposed to the ambient atmosphere of Titan.

[16] Figure 3 shows the dynamic pressure, ambient pressure, and descent velocity versus time from sampling initiation at 147 km. The ambient pressure, mass density, and descent velocity data are from the HASI experiment [*Fulchignoni et al.*, 2005] and the Descent Trajectory Working Group [*Kazeminejad et al.*, 2007]. The dynamic pressure shown in Figure 3 (P_d) was not measured directly. It was computed using the familiar relation, $P_d = 1/2\rho V^2$, where ρ is the in situ mass density of the atmosphere and V is the descent velocity. The abrupt change of the dynamic pressure occurred when the descent velocity increased after jettison of the second parachute.

2.2. Measurement Sequence

[17] The measurement sequence was preprogrammed. The atmosphere was sampled nearly continuously during the entire descent, interrupted only when the contents of the noble gas and the sample enrichment cells were analyzed and when ACP samples were transferred. GC samples were collected in storage volumes in the upper atmosphere for later analysis when the descent slowed and more time was available for analysis. At lower altitudes, close to the surface, GC samples were injected directly from the atmosphere.

[18] The measurement sequences are shown in Figure 4. The change of the ambient pressure and temperature are shown in Figure 4a. The ambient pressure and temperature were measured by the HASI experiment [*Fulchignoni et al.*, 2005]. The events in ion source 1 are indicated in Figure 4b, and the times when ACP samples were analyzed are shown in Figure 4c. Finally, the GC sample collection and analysis times of the batch samples with ion sources 3, 4, and 5 as detectors are plotted in Figure 4d.

[19] The mass spectrometer was scanned continuously in unit mass steps over the mass range (m/z = 2–141) with a dwell time of 4.592 ms per step. Periodic high-resolution spectra, eight steps per unit mass, were taken to verify correct mass tuning. With a small time fraction allowed for settling of transients after each sample step, the period of a full unit mass scan cycle was 937.5 ms. In-flight, the time doubled to 1.875 s between samples because the instrument data stream was split on two quasi-redundant transmission links from the Huygens probe to the Cassini orbiter, and one receiver channel was inadvertently not turned on.

[20] The preprogrammed measurement sequence was properly executed during the mission. Ion source 5, which served as a detector for the N_2-CO separation column failed to operate normally at 74 km altitude. This resulted in the loss of the data from this column and the measurement of

the CO concentration. A simultaneous sensitivity change of ion source 1 occurred, likely related to the ion source 5 failure. The sensitivity change was mass independent, which is consistent with a bias potential change at one or more of the ion focusing lenses. This did not affect the mole fraction and isotope data, since absolute ambient partial pressure measurements by the GCMS were not intended. Large atmospheric turbulence affected the probe motion at the same time, and it likely triggered the event. The exact cause of that failure in the instrument could not be determined, but an examination of the housekeeping data pointed to an electrical malfunction in the ion source supply circuit.

[21] As indicated in Figure 4, data were collected from 146 km altitude to the surface for 8871 s (2 h and 27 min). From 146 to 65 km, only atmospheric gases were analyzed directly, introduced through leak L1 into ion source 1. Direct atmosphere sampling was interrupted for 6 min from 65 to 56 km to analyze the contents of the noble gas scrubber cell followed by the analysis of the content of the sample enrichment cell. The gas samples for the scrubber and enrichment cell were collected from 77 to 75 km. Direct atmosphere sampling was resumed at 56 km altitude using the second, lower conductance, leak L2 for ion source 1. The GC analysis was also initiated at this time scanning ion sources 3, 4, and 5. Ion source 2 was operated for two short periods for the analysis of the transferred ACP samples. The probe and the instrument survived the surface impact, although this was not an objective of the mission. Data were collected for an additional 70 min from gases evaporating from the surface.

[22] The ion arrival rate at the detector during each measurement step constituted the primary measurement. Pulse counting rates per time sample varied from 0 to an equivalent of 10^8 counts/s. Because of pulse pile up and a finite recovery time of the pulse counting system after a pulse was received, a correction needed to be applied to the raw count rates up to 7×10^6 counts/s. The corrected count rate was derived from the expression

$$[R] = [n]/(1 - [n][T]), \quad (1)$$

where $[R]$ is the corrected count rate and $[n]$ is the measured count rate. The value of $[T]$ was empirically determined as 2.8×10^{-8} s using cruise checkout data from the background argon present in the sensor at that time.

[23] At pulse count rates higher than 7×10^6 counts/s the correction could no longer be applied. In that case a proxy mass peak can be used such as the fractionation peak of the parent mass peak, which is at a lower magnitude. This occurred only for molecular nitrogen where the N^+ peak, at $m/z = 14$, with a peak height ratio of 0.0467 relative to the parent $m/z = 28$ peak, was used as a proxy for the $m/z = 28$ peak. This ratio was determined from dead time corrected flight data when both pulse count rates were sufficiently low in signal to allow the determination (from 100 to 1000 s descent time). The results were consistent with the laboratory calibration data.

[24] Data rate limitations for the link between the Huygens probe and the Cassini orbiter restricted the available data rate for the GCMS to 1770 bits/s for combined science and housekeeping data. To cover the full range of available data from the instrument, it was necessary to compress the data. Square root data compression was chosen for this purpose. Maximum resolution for low count rate science data from the detector was maintained, however, by transmitting counts uncompressed from 0 to 127 counts per integration period (0–27,657 counts/s).

[25] Figure 5a shows sample mass spectra from the stratosphere averaged from ~130 to 120 km altitude and ~4 to 6 hPa ambient pressure, Figure 5b from the troposphere at ~20 to 10 km altitude and ~500 to 900 hPa ambient pressure, and Figure 5c from the surface at 1500 hPa.

2.3. Calibration

[26] The instrument was calibrated on a dynamic flow system where the time, ambient pressure, and ambient temperature profile were simulated as expected during the descent of the Huygens probe. *Niemann et al.* [2002] have described details of the calibration facility and the calibration process. The objective of the calibration was to determine the overall system transfer characteristics for molecular species expected to be in the atmosphere of Titan. The transfer function of the instrument is species dependent. The transmission of the gas mixtures through the capillary leaks is pressure dependent and mole fraction dependent. The ionization cross sections and, to a lesser degree, the conversion efficiencies of the ion detector are species dependent. The effective pumping speeds of the vacuum pumps are different for inert and reactive gases. Although the vacuum pumps were conductance limited, i.e., their effective pumping speed was nearly constant for the time of the descent and on the surface, the specific pump properties needed to be determined. While the getters pump reactive gases only, except methane, the sputter ion pumps remove all gases, and hence, the mole fraction in the ion source was different from that of the ambient atmosphere.

[27] Static calibration runs were conducted with hydrocarbon mixtures and noble gas mixtures, introduced at several fixed pressure levels. Dynamic descent simulations verified the system response prior to instrument delivery for flight.

[28] The calibration of the flight instrument was not completed before launch. Limitation of the lifetime of the chemical getters and the sputter ion pumps, which needed repeated replacement during the calibration period required more time than was available before launch. After Titan encounter, work continued on the flight spare unit, which was built to be identical to the flight instrument. The effect of unavoidable differences between the two instruments on the measurement accuracies is assumed to be small. The calibration data are expressed as pressure-dependent calibration factors. The dead time and background corrected count rates of ions are multiplied by the calibration factors to produce the mole fractions of species in the ambient atmosphere. Calibration factors are pressure dependent because transmission of molecular species through the capillary leaks depends on the molecular properties, mass and viscosity, and on the mole fractions. The diameter and length of the capillaries needed for correct pressure reduction from the ambient pressure to the ion source pressure resulted in the gas flow through the capillaries to be in the transition regime between free molecular and viscous flow.

[29] Calibration data were obtained for CH_4 and H_2 in N_2 using certified premixed gas mixtures of 2%, 5%, and 10%

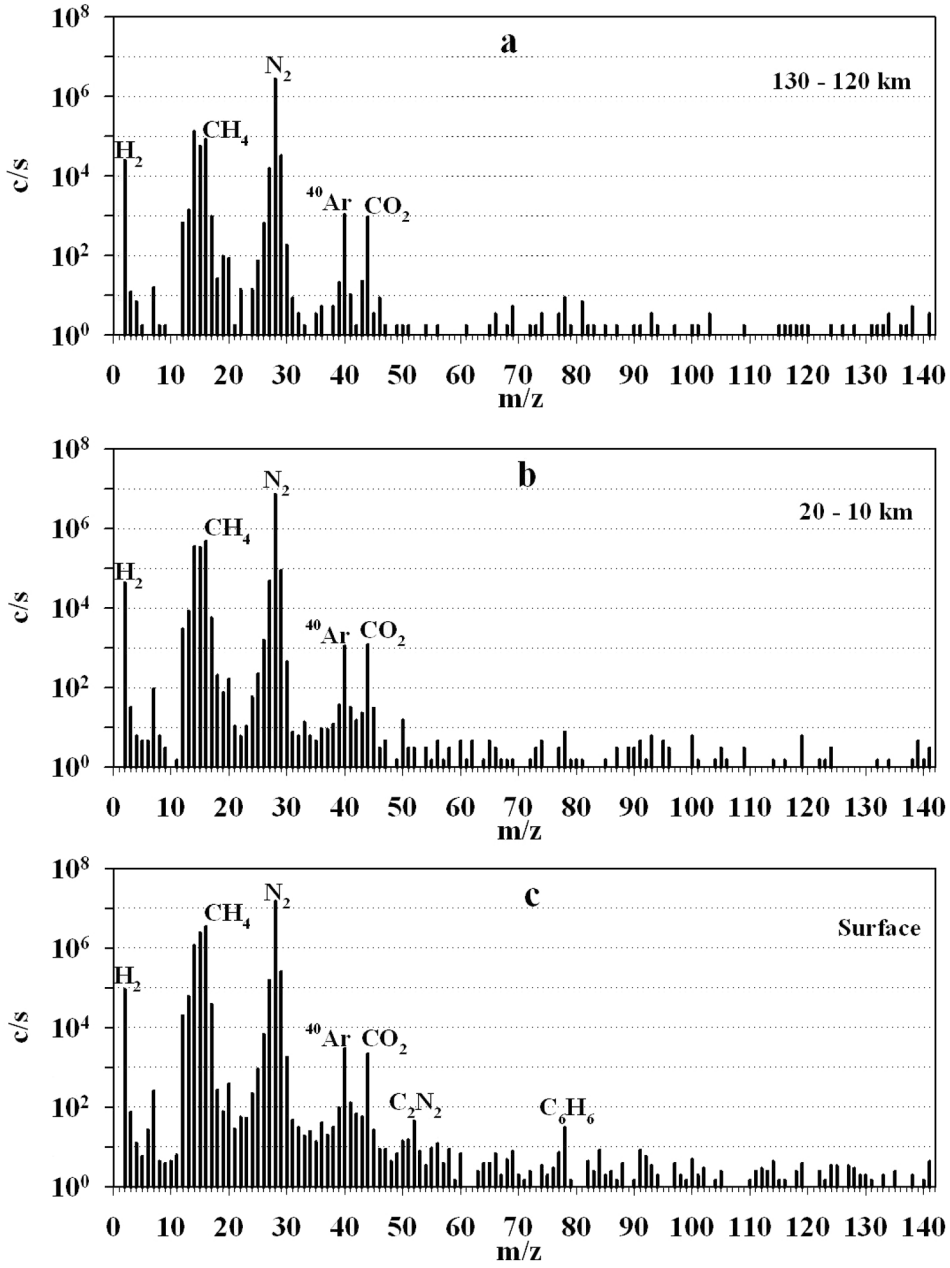

Figure 5. Examples of averaged mass spectra obtained at high and low altitude and on the surface. (a) Average from 130 to 120 km, ~4 to 6 hPa ambient pressure (leak L1). (b) Average from 20 to 10 km, ~500 to 900 hPa ambient pressure (leak L2). (c) Average surface spectra (leak L2) from 9000 to 13,000 s.

methane and 1% and 3% hydrogen in molecular nitrogen. When normalized, the differences in the calibration results for the different mole fractions were smaller than the calibration errors. Polynomials were fitted to the calibration curves and were applied to the flight data. For gas species not directly calibrated in either the flight unit or flight spare unit, literature ionization cross sections were used relative to N_2.

[30] The laboratory calibration data showed an inconsistency between the flight and the flight spare instrument in the system pump down of hydrogen. This was observed during the transition period from the leak L1 to the leak L2 measurement phase when ion source 1 was isolated from the atmosphere for 90 s for pump down to remove residual gases from the leak L1 operating period. Different from the results for all other gases, the hydrogen remained at a higher background level in the flight unit than what was observed before flight and in the flight spare unit in the laboratory. The discrepancy can be resolved if it is assumed that the getter pumps for ion source 1 in the flight instrument did not pump hydrogen during the descent and only the sputter ion pump was effective for ion source 1. This would be possible

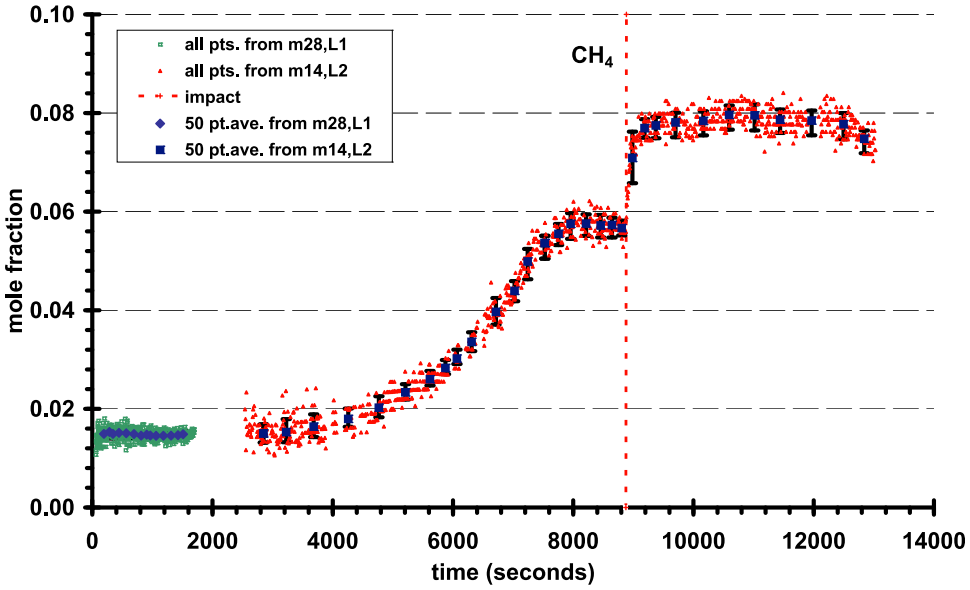

Figure 6. Methane mole fraction all sample points, diamonds, and squares averaged over 50 sample points versus time from sequence initiation. The analysis was divided into regions for leak L1 and leak L2. N_2 m/z = 14 counts (corrected for methane contribution) are a proxy for m/z = 28 for the leak L2 data because at lower altitudes the pulse counts at m/z = 28 are no longer valid. The regions are marked in the figure and the legend. The time of surface impact is also marked. The error bars are the standard deviation.

if a small hydrogen leak in the isolation valve from the gas chromatograph hydrogen reservoir to the sample inlet system had developed during or shortly after launch. The leak rate would have been too small (less than 1×10^{-6} std.cc/s) to detect after launch, but over a time of 7 years would have gradually saturated the getters of ion source one.

[31] Since the gettering process for hydrogen is different from the other gases (going into solution reversibly rather than chemical bonding), the hydrogen present in the getter has only a small effect on the pumping speed of the getters for the other gases. The hydrogen loading on the getters for the other ion sources was only small because they are decoupled and the gas flow from the sample inlet system is 6 orders of magnitude lower than the flow to the getters in ion source 1. However, the getter in the noble gas and sample enrichment cells was also exposed to a higher gas flow. The possible effect on the enrichment cell data is still being evaluated. The assumption is also consistent with theoretical and experimental data obtained in our laboratory of the getter capacities and equilibrium vapor pressure values for the getter mass and material. With that caveat the hydrogen data are presented with the assumption that the hydrogen in ion source one was pumped by the sputter ion pump only. The ratio of the total pumping speed, with fully activated getters, to that of the sputter ion pump only was determined to be 9.02 in the laboratory calibration for the flight spare instrument. The indicated H_2 mole fraction was corrected by that factor. Since it cannot be determined with certainty, based on the flight and laboratory calibration data, that the effective pumping speed for hydrogen of the ion source 1 getter in the flight instrument was exactly zero, the hydrogen mole fraction presented is considered to be a the lower limit.

[32] Ambient pressure data from the HASI experiment [*Fulchignoni et al.*, 2005] and the Descent Trajectory Working Group [*Kazeminejad et al.*, 2007] were used to correlate the flight data with the calibration data.

[33] Simulation experiments of the interaction of the instrument sample inlet line with the surface are needed for a more thorough understanding of the data obtained on the surface of Titan.

3. Data

3.1. Methane

[34] As already observed from the ground for methane [*Kuiper*, 1944] and from Voyager 1 for nitrogen [*Broadfoot et al.*, 1981; *Tyler et al.*, 1981], molecular nitrogen (N_2) and secondarily methane (CH_4) are the major constituents of the atmosphere of Titan. The GCMS measurements confirmed this and determined the mole fraction of methane from 140 km altitude to the surface during the probe descent.

[35] In the mass spectra received during the descent, the contributions to the mass peak intensities at m/z = 28 and 16 were primarily from N_2 and CH_4, respectively. Contributions from other species were negligible because their parent peak intensities were much lower.

[36] Calibration data were applied as described in section 2.3. At m/z = 14, the peak intensity needed to be corrected for the contribution from methane fractionation in the ion source, $^{12}CH_2^+$. The fraction was 0.0506 of the m/z = 16 (CH_4) count rate. It was determined from the noble gas scrubber cell data obtained in-flight where methane was the only nonnoble atmospheric gas that was not removed by the chemical getters.

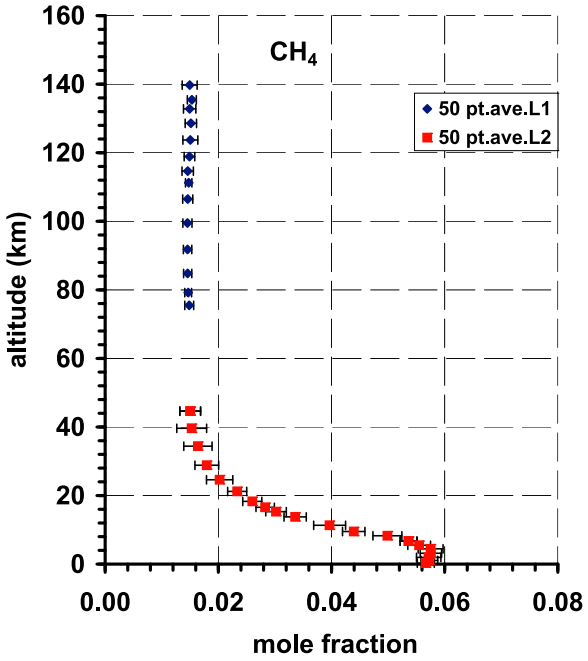

Figure 7. Methane mole fraction averaged over 50 sample points versus altitude. The error bars are the standard deviation. Leak L1 data are blue diamonds, and leak L2 data are red squares.

[37] The mole fractions were computed using

$$CH_4/(N_2 + CH_4) = \frac{[16]/[28]/[cf_{16,28}]}{1 + [16]/[28]/[cf_{16,28}]} \quad (2)$$

or where $m/z = 14$ due to N_2 is used as a proxy for $m/z = 28$,

$$CH_4/(N_2 + CH_4) = \frac{[16]/[14]/([28]/[14]_r)/[cf_{16,28}]}{1 + [16]/[14]/([28]/[14]_r)/[cf_{16,28}]}, \quad (3)$$

where [16], [28], [14] are the actual pulse count rates at the respective mass values, corrected for dead time. Residual background counts were subtracted. $[cf_{16,28}]$ is the calibration factor for the CH_4/N_2 ratio. $[28]/[14]_r$ is the dead time corrected count ratio at $m/z = 28$ and 14 in the range where both are valid.

[38] The results are shown in Figure 6 as function of time from sequence initialization. The section where the mass 14 proxy was used is marked in red. To improve the statistical accuracy, data points were averaged over approximately 50 sample points also shown in Figure 6. The error bars show the standard deviation. The vertical red dashed line marks the time of surface impact. The variation of the mole fraction with altitude is shown in Figure 7. A gradual increase in the mole fraction is noticed starting at 3000 s, about 40 km above the surface, to 7500 s and about 7 km above the surface. It then remained nearly constant until surface impact. After landing, it again increased rapidly and remained nearly constant until close to the end of the data transmission (Figure 6). The time-averaged numerical data as shown in Figures 6 and 7 are tabulated in Table 1. The errors shown are one sigma statistical errors only. Additional systematic errors resulting from calibration and differences between the flight instrument and the flight spare instrument are estimated to be ±5%.

[39] The increase of the mole fraction with decreasing altitude down to approximately 7 km is evidence for cloud formation (see section 4.1) and, after landing on the surface, of evaporation of methane from the soils beneath the heated probe.

3.2. Nonmethane Hydrocarbons and Other Trace Gases

[40] Hydrocarbons of C_2 and higher order and nitrogen containing species were not reliably detected above the surface by the GCMS. Numerous heavy hydrocarbons and nitriles, produced by photochemical reactions and energetic particle collisions, however, were detected in situ at ionospheric altitudes above 900 km by the Cassini ion and neutral mass spectrometer (INMS) [*Waite et al.*, 2007] during Titan flybys of the Cassini orbiter and in the stratosphere remotely by the Cassini composite infrared spectrometer (CIRS) [*Coustenis et al.*, 2007]. As the newly formed species descend, they undergo additional chemical reactions to form more complex compounds and aerosols while their parent mole fractions decrease. Ultimately, most gases condense or change to aerosols as they reach the tropopause due to the decreasing temperature with decreasing altitude between the stratosphere and troposphere [*Wilson and Atreya*, 2004].

[41] When the GCMS measurements were initiated (below 146 km), only traces of C_2H_6 and C_2H_2 were near the detection threshold of the instrument but could not be quantified. Evaporation of these materials from the surface was observed, however, after the probe landed. In Figure 5c, the mass spectra show more high mass peaks on the surface. Still most of the count rates at higher mass values are close to the detection threshold and only a few mass peaks stand out.

[42] The probe came to rest on the surface in an upright position. In this position, the sample inlet port of the GCMS could have been touching the surface or was inside of a small cavity around the inlet port created by the settling motion. The interface geometry of the inlet sample port and the surface is illustrated in the drawing shown in Figure 8. The sample inlet line heated the inlet port on the surface either by conduction (direct contact) or by conduction and radiation through the surrounding atmosphere. The exact nature of the thermal contact of the inlet port with the surface is not known nor is the exact temperature or temperature distribution known of the surrounding surface area. It can, however, be safely assumed that the temperature inside the probe and downstream in the sample line was higher than the temperature of the surface and in the vicinity of the capillary leak. The temperature at the entrance port of the inlet tube was not monitored. On the surface, a value of 140 K was estimated from temperature modeling of the sample inlet line [*Lorenz et al.*, 2006].

[43] The inlet port temperature, being higher than the ambient temperature, caused the evaporation of low boiling point surface condensates followed by convective gas flow through the heated sample line. In addition to methane, which showed the highest evaporation rate and fastest time response, a number of other species were also evaporating at different rates and with different starting times. This is

Table 1. CH_4 Mole Fraction, 50 Data Point Averages

	Time From Entry (s)	10^2 Mole Fraction	10^3 Standard Deviation	Altitude (km)	Pressure (hPa)	Temperature (K)
	193	1.49	1.32	139.8	3.3	162.8
	285	1.53	0.79	135.5	3.7	161.1
	344	1.49	1.09	132.8	4.0	161.0
	443	1.51	1.00	128.6	4.4	157.2
	565	1.51	1.32	123.7	5.0	156.1
	693	1.49	0.94	118.9	5.7	155.0
	813	1.46	1.01	114.7	6.4	152.6
Leak 1	905	1.48	0.57	111.2	6.9	148.7
	965	1.46	0.89	106.5	7.6	148.4
	1061	1.45	0.80	99.5	9.6	144.8
	1183	1.46	0.74	91.8	12.2	139.6
	1310	1.46	0.72	84.8	15.3	132.7
	1425	1.47	0.60	79.2	18.5	125.5
	1510	1.49	0.79	75.5	21.2	118.9
	Average Leak1	**1.48**	0.90			
	2846	1.50	1.83	44.6	112.8	70.5
	3226	1.53	2.64	39.6	155.2	70.7
	3683	1.64	2.49	34.4	214.4	71.4
	4259	1.80	2.10	28.9	302.4	73.0
	4766	2.02	2.32	24.6	390.7	74.9
	5210	2.33	1.69	21.2	477.0	76.8
	5617	2.60	1.68	18.3	563.2	78.5
	5874	2.83	1.62	16.6	620.9	79.6
	6065	3.02	1.82	15.3	665.8	80.4
	6310	3.36	1.96	13.8	724.9	81.4
	6715	3.97	2.82	11.3	827.4	83.2
Leak 2	7023	4.39	1.98	9.5	909.4	84.4
	7242	4.99	2.56	8.3	969.9	85.4
	7527	5.36	1.48	6.7	1051.4	86.8
	7756	5.55	2.01	5.5	1118.4	87.8
	7956	5.75	2.20	4.5	1178.3	88.8
	8214	5.76	1.89	3.2	1257.2	90.0
	8457	5.72	2.16	2.0	1333.7	91.2
	8644	5.73	1.48	1.1	1393.8	92.3
	8807	5.67	1.50	0.3	1446.7	93.1
	8985	7.09	5.35	0.0	1467.0	93.7
	9188	7.69	1.85			
	9374	7.75	1.73			
	9701	7.81	1.97			
	10164	7.84	1.96			
	10594	7.96	1.93			
	11018	7.95	2.25			
	11441	7.86	2.08			
	11966	7.85	2.05			
	12497	7.77	2.26			
	12840	7.48	1.72			
	Average Leak2 From 6.7 km to surface	**5.65**	1.82			

shown in Figure 9. Increases in vapor concentrations after landing were identified for C_2H_6, C_2H_2, and C_2N_2, in addition to CH_4. A small increase in the C_6H_6, $m/z = 78$, 51, and 50 mass peaks also occurred, but it could not be identified unambiguously as originating from the surface. C_6H_6 was permanently present in the instrument as a trace background gas and the observed very small increase, which occurred before impact, could have been surface outgassing from the sampling system stimulated by the incoming atmospheric gas. The upper limit for the C_6H_6 mole fraction is 1×10^{-7}. The list above is ordered in decreasing level of confidence of correct species identification. Pulse count rates were used from either parent and/or fractionation peaks, and with application of the respective calibration factors, mole fractions were calculated. All reached quantifiable levels only after landing. The dashed vertical lines indicate the time of surface impact. The finite values above the surface seen in the figures are residuals at the detection threshold and are not valid numerical quantities. The detection threshold for C_2H_6 and C_2H_2 is relatively high with respect to the full dynamic range of the instrument because the mole fractions were derived by subtracting pulse count rates of interfering species from the total at $m/z = 30$ and 26, respectively, to obtain the plotted values. The upper limits of the mole fractions of the species in the atmospheric portions during the descent are estimated to be 1×10^{-5} for C_2H_6, 2×10^{-6} for C_2H_2, and 1×10^{-7} for C_2N_2.

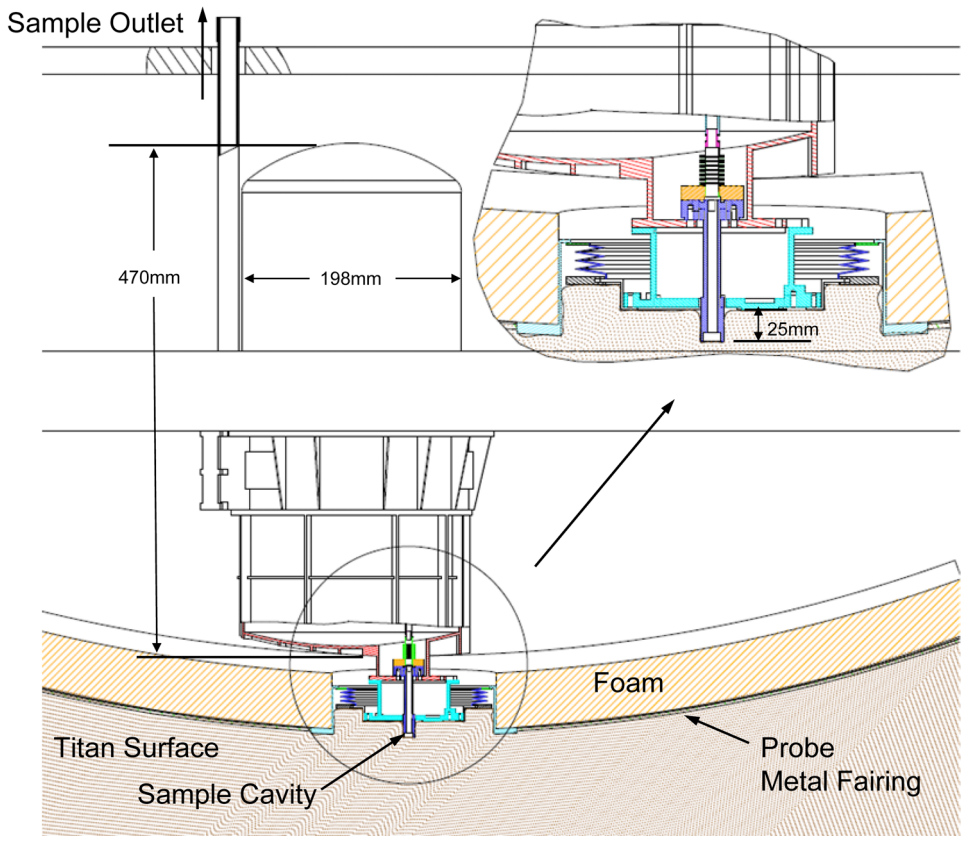

Figure 8. A schematic of the GCMS sample inlet and its mounting in the Huygens probe.

3.3. Carbon Dioxide

[44] Carbon dioxide, CO_2, is not expected to be present in any detectable abundance in the lower atmosphere of Titan. Evaporation from the surface, from CO_2 ice, is plausible and was observed from monitoring the peak intensity at $m/z = 44$. The $m/z = 44$ peak contained also contributions from a constant CO_2 background in the ion source and from propane, C_3H_8. Contributions from propane can be separated by observing the fractionation peaks of propane at $m/z = 43$ and 42. The CO_2 background, where measured, was constant and was subtracted. The result for CO_2 versus time is shown in Figure 9. Surface impact time is indicated in Figure 9 by a vertical dashed line. As with the solid organic compounds on the surface the CO_2 mole fraction monotonically increases with time until the end of data transmission.

3.4. Hydrogen

[45] Molecular hydrogen in the atmosphere was detected by the GCMS by observing the count rates at $m/z = 2$. The mole fraction was then calculated using the relation,

$$H_2/(N_2 + CH_4) = \frac{([2] - [16][cf_{2,16}])/[28]/[cf_{2,28}]}{1 + [16]/[28]/[cf_{16,28}]}. \quad (4)$$

When the $m/z = 28$ counts were saturated, the counts at $m/z = 14$ were used as proxy for mass 28 (corrected for CH_4 contributions),

$$H_2/(N_2 + CH_4) = \frac{([2] - [16][cf_{2,16}])/[14]/([28]/[14]_r)/[cf_{2,28}]}{1 + [16]/[14]/([28]/[14]_r)/[cf_{16,28}]}, \quad (5)$$

where [2], [16], [28], and [29] are the pulse count rates at the respective mass values, corrected for dead time, GC H_2 carrier gas cross talk (leak L2 only) and residual ion source background counts. $[cf_{2,28}]$ is the calibration factor for the H_2/N_2 ratio at $m/z = 2$ to $m/z = 28$. $[cf_{16,28}]$ is the calibration factor for the CH_4/N_2 ratio at $m/z = 16$ to $m/z = 28$ and $[28]/[14]_r$ is the dead time corrected count ratio at $m/z = 28$ and 14 in the range where both are valid.

[46] Contributions to the $m/z = 2$ count rate from dissociative ionized H_2^+ ions of CH_4 were evaluated from laboratory calibration with CH_4 using the flight spare instrument.

[47] The H_2^+ ion fraction of the CH_4^+ ion count rate was

$$[cf_{2,16}] = [2]/[16]_{lab} = 1.05 \times 10^{-3}. \quad (6)$$

Species other than N_2 and CH_4 were not included in the mole fraction calculations. Their contributions are negligible compared to other measurement errors.

[48] The fixed (static) background in the ion source was determined for the leak L1 region before the sample inlet system was opened to the atmosphere. Fixed background contributions in the leak L2 region were determined at the

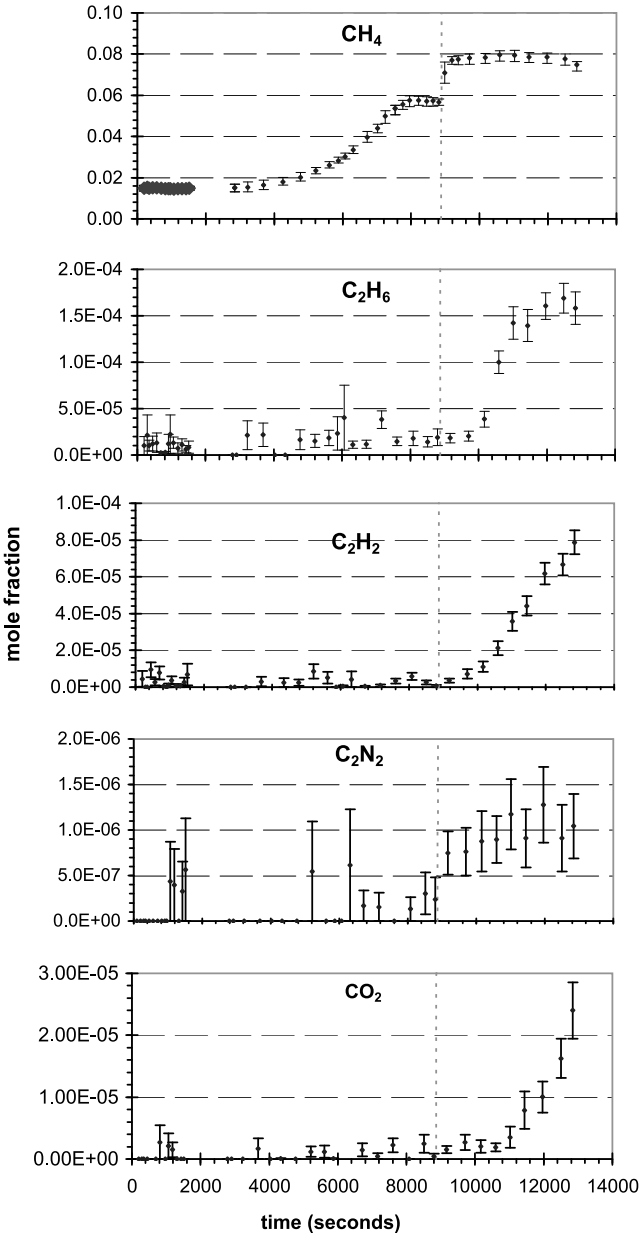

Figure 9. Mole fractions of CH_4, C_2H_6, C_2H_2, C_2N_2, and CO_2 versus descent time. Error bars are standard deviation. The time of surface impact is indicated by a vertical dashed red line.

beginning of the leak L2 measurement phase when ambient hydrogen contributions were negligible. The carrier gas contribution was determined by observing the increase in the $m/z = 2$ count rate at the time when the hydrogen gas flow was started. It results from cross talk of the hydrogen pressure in the GC dedicated ion sources 3, 4, and 5 into ion source 1. The increase was of the order of the residual ion source background. It does not vary with time since the carrier gas pressure and hence the pressures in the GC dedicated ion sources were constant. Contributions from other hydrogen carrying compounds were negligible.

[49] The calibration factor $[cf_{2,28}]$ was determined from laboratory calibration of the flight spare instrument with representative gas mixtures of H_2, CH_4, and N_2. As described in section 2.3, this calibration factor includes the pressure and mole fraction-dependent transmission through the capillary leak arrays of species with different molecular weight, the ionization cross sections, the ion transmission through the mass filter and ion lens system, and conversion efficiency of the secondary electron multiplier ion detector. The calibration factor was expressed in a closed form by fitting the laboratory calibration data as function of pressure.

[50] The mole fraction of hydrogen versus time from entry (all sampling points) is shown in Figure 10 for the high-altitude region (144–66 km), leak L1, and the low-altitude and ground region (45 km to the ground), leak L2. Averaged data over approximately 50 sample points are also presented in Figure 10. The error bars shown are the standard deviations. Figure 11 shows the altitude dependence of the mole fractions. On the surface, the mole fraction remains constant until about 10,000 or 1300 s after impact. The mole fraction then decreases gradually until the end of the mission. Similar gradual decrease in mole fraction was observed also for methane. The cause is not explained at this time. An instrument effect or a gradual change in the gas flow through the sample inlet line because of the changes in temperature over time could be contributing. The 50-point average data are tabulated in Table 2.

3.5. Noble Gases

[51] ^{36}Ar and ^{22}Ne were the only nonradiogenic or "primordial" noble gases detected by the instrument and only in sufficient abundance in the noble gas cell for quantitative evaluation. Interference with peaks produced by organic molecules makes it impossible to isolate them in the direct measurement sequence during the descent.

[52] Noble gas cell data were collected during the descent from 77 to 75 km and analyzed during the descent from 64 to 61 km. Figure 12 shows the mass spectrum from the noble gas cell. The function of the noble gas cell was to remove or significantly reduce the concentration of the reactive gases in the cell that minimized the mass spectral interference from these gas species and enhanced the noble gas concentration relative to molecular nitrogen. This was accomplished with a chemical getter that pumped all reactive gases except methane. Mixing ratios of the noble gases with respect to methane in the cell were then converted to mole fractions using the methane mole fraction measured at the time when the noble gas and enrichment sample collection occurred. More details on the operation of the noble gas cell can be found in the work of *Niemann et al.* [2002]. Molecular nitrogen was only reduced in concentration. It could not be removed completely from the cell. The pumping capacity of the getter is not sufficient to remove all nitrogen. Carbon dioxide (CO_2), benzene (C_6H_6), and some other traces in the low mass range were permanent background gases in the ion source, which could not be removed during the preflight processing. They did not originate from the cell. Molecular hydrogen was not removed because of the diminished getter pumping presumably due to the gas leak from the GC carrier gas reservoir as described in section 2.3.

[53] As in all other cases, laboratory calibration data for the instrument transmission function were applied involving ionization cross sections, pulse counter dead times, gas

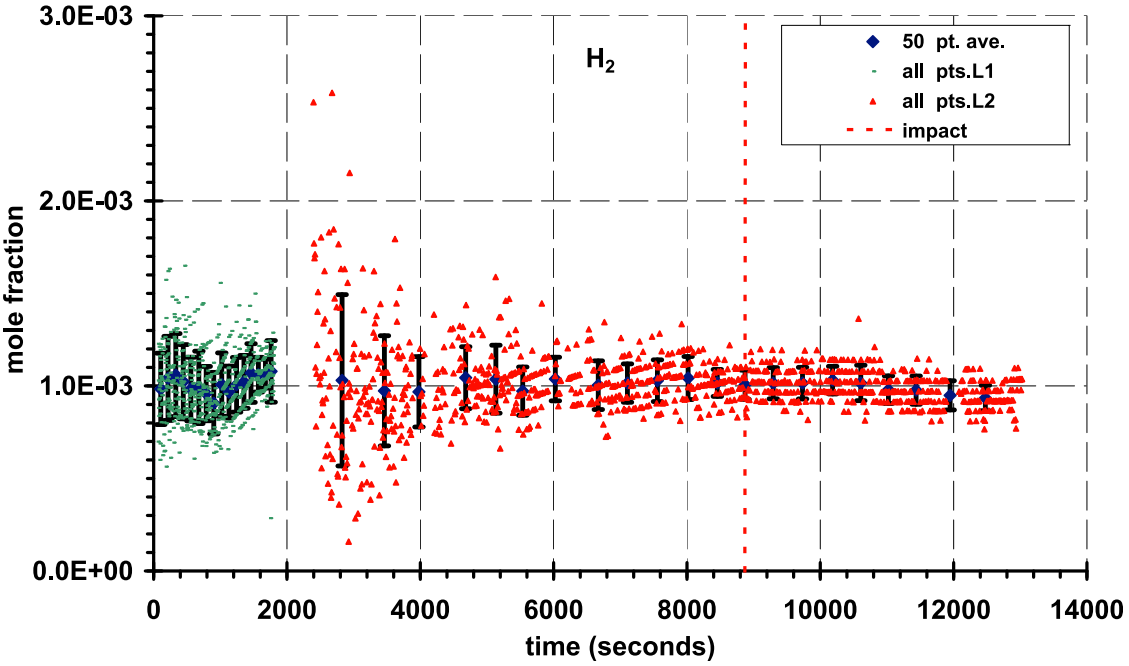

Figure 10. The mole fraction of molecular hydrogen versus time from sequence initiation. All data point and 50 sample point averages are shown for the leak L1 and leak L2 regions. The error bars are standard deviations. The time of surface impact is indicated by a vertical dashed red line.

conductance of capillary leaks, and effective pumping speed.

[54] The ^{36}Ar mole fraction from the noble gas cell data is

$$^{36}\mathrm{Ar}/(\mathrm{N_2} + \mathrm{CH_4}) = (2.1 \pm 0.8) \times 10^{-7}. \quad (7)$$

The presence of ^{38}Ar was confirmed qualitatively. The small number of pulse counts collected was approximately correct for an isotope ratio for ^{38}Ar/^{36}Ar of 0.2. It also provided assurance that the mass peak at $m/z = 36$ was not a residual hydrocarbon peak. The ^{38}Ar upper limit is $\sim 5 \times 10^{-8}$.

[55] The mole fraction of ^{20}Ne could not be determined at $m/z = 20$. Much larger peaks of doubly ionized ^{40}Ar mask the peaks. The upper limit of the mole fraction for ^{20}Ne is $\sim 2 \times 10^{-5}$.

[56] The detection threshold of the isotope ^{22}Ne was also raised because of doubly ionized CO_2 background interference at the $m/z = 22$ peak. Although the interference peak value was of the same order as the total peak count value ($^{22}Ne^{+}$ and CO_2^{++}), it could be subtracted from the total.

[57] The remaining pulse count values were converted to a mole fraction of ^{22}Ne,

$$^{22}\mathrm{Ne}/(\mathrm{N_2} + \mathrm{CH_4}) = (2.8 \pm 2.1) \times 10^{-7}. \quad (8)$$

This result should be considered tentative because the signal level is low, close to the detection threshold at $m/z = 22$, which is also reflected in the large statistical error shown.

[58] Doubly ionized ^{20}Ne at $m/z = 10$ and ^{22}Ne at $m/z = 11$ were not detected. They occur in an interference-free region, but their intensity would still be below the detection threshold of the instrument.

[59] CO_2 resided in the ion source as low-level permanent background gas. It is a common contaminant in-flight mass

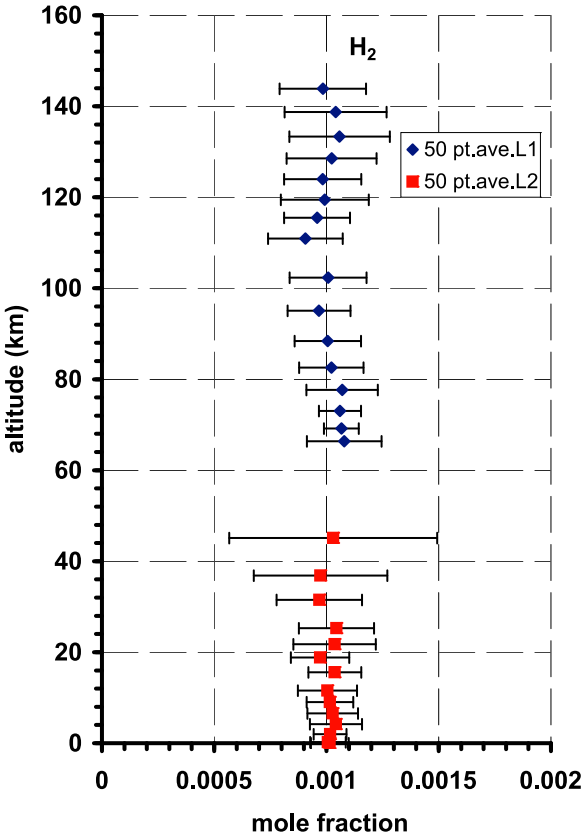

Figure 11. The mole fraction of molecular hydrogen versus altitude. The data points shown are 50 sample point averages. The error bars are standard deviations.

Table 2. H_2 Mole Fraction, 50 Data Point Average

	Time From Entry (s)	10^3 Mole Fraction	10^4 Standard Deviation	Altitude (km)	Pressure (hPa)	Temperature (K)
	107	0.98	1.93	143.9	3.0	166.5
	214	1.04	2.27	138.7	3.4	162.4
	332	1.06	2.24	133.4	3.9	160.9
	444	1.02	2.00	128.6	4.4	157.2
	558	0.98	1.72	124.0	5.0	156.1
	678	0.99	1.96	119.5	5.6	155.3
	788	0.96	1.47	115.5	6.3	153.4
	902	0.91	1.66	110.9	6.9	149.2
Leak 1	1021	1.01	1.72	102.3	8.7	146.5
	1130	0.97	1.40	95.1	11.0	141.8
	1244	1.01	1.48	88.4	13.6	136.7
	1355	1.02	1.43	82.6	16.5	130.2
	1460	1.07	1.59	77.7	19.6	122.7
	1571	1.06	0.94	73.0	23.3	114.1
	1676	1.07	0.78	69.2	27.3	102.8
	1762	1.08	1.66	66.4	31.0	90.5
	Average Leak 1	**1.01**	1.64			
	2827	1.03	4.63	45.1	112.3	80.4
	3461	0.97	2.98	36.8	184.4	70.9
	3978	0.97	1.90	31.5	258.5	72.2
	4680	1.04	1.67	25.3	374.9	74.6
	5133	1.04	1.83	21.8	461.4	76.5
	5536	0.97	1.30	18.9	545.6	78.1
	6026	1.04	1.18	15.6	657.1	80.2
	6669	1.00	1.31	11.6	815.5	83.0
	7106	1.02	1.04	9.0	932.4	84.8
	7556	1.03	1.13	6.6	1060.1	86.9
Leak 2	8018	1.04	1.16	4.2	1197.1	89.1
	8456	1.02	0.73	2.0	1333.4	91.2
	8872	1.01	0.79	0.2	1450.9	93.5
	9294	1.01	0.84	0.0	1467.6	93.7
	9733	1.02	0.85			
	10185	1.03	0.75			
	10607	1.02	0.96			
	11022	0.98	0.75			
	11437	0.98	0.76			
	11947	0.95	0.79			
	12476	0.93	0.69			
	Average Leak 2 Above surface	**1.01**	1.67			

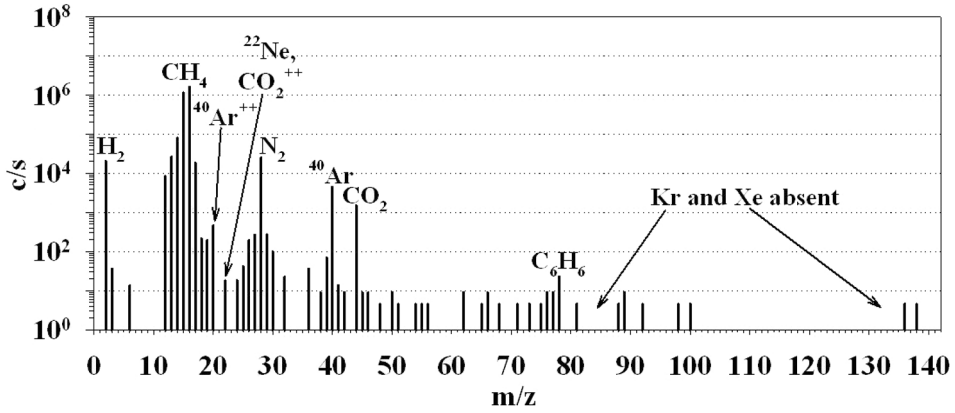

Figure 12. Average mass spectrum of the rare gas cell contents. CO_2 (at $m/z = 44$) and C_6H_6 (at $m/z = 78$) were permanent background gases in the ion source.

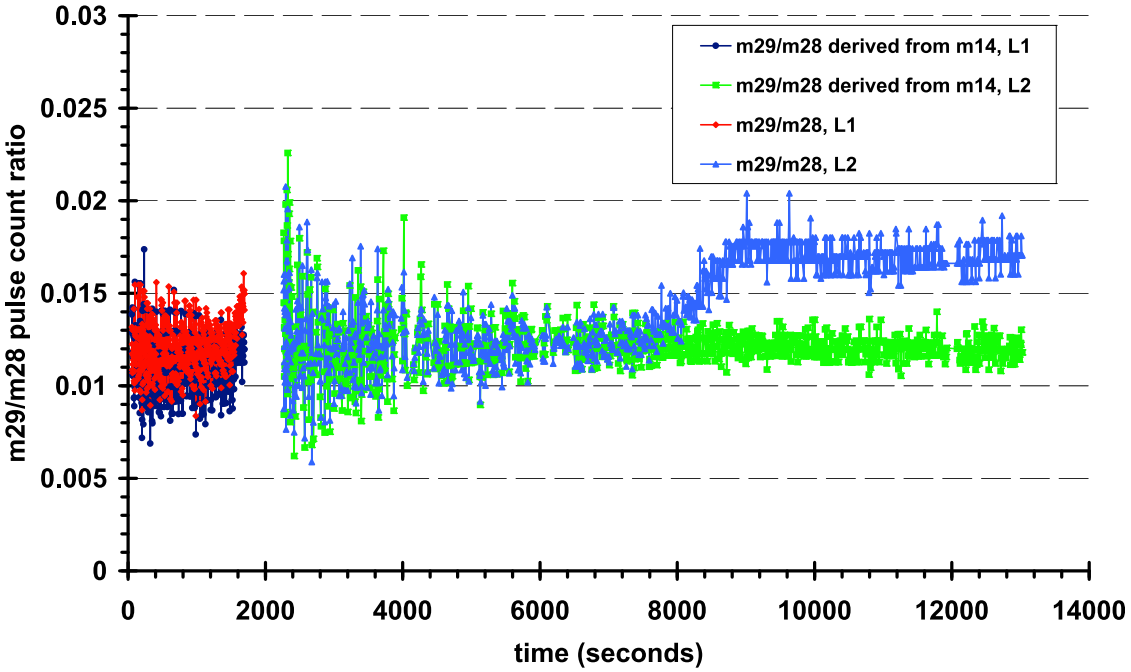

Figure 13. Pulse count ratios of $m/z = 29$ ($^{15}N^{14}N^{+}$) to $m/z = 28$ ($^{14}N_2^{+}$) (red and blue) and $m/z = 29$ to $m/z = 14$ proxy (black and red) versus time from sequence initiation shown for the leak L1 and leak L2 regions. The increase in the $m/z = 29$ to $m/z = 28$ count ratios at ~1500 and 7000 s results from counter saturation at high count rates for $m/z = 28$.

Table 3. Isotope Ratios and Noble Gas Abundances

Isotopes	Derived From	Ratios	Altitude Range	Ion Source 1 Gas Inlet Leak
$^{14}N/^{15}N$	$^{14}N_2$, $^{14}N^{15}N$	167.4 ± 0.6	144–77 km	Leak 1
		168.0 ± 2.6	47–32 km	Leak 2
		167.6 ± 1.3	24–16 km	Leak 2
		167.7 ± 0.6	average of all	
$^{12}C/^{13}C$	$^{12}CH_4$, $^{13}CH_4$	91.6 ± 1.9	127–67 km	Leak 1
		91.7 ± 1.5	76.5 km (noble gas cell)	Leak 3
		90.6 ± 1.0	23 km to surface	Leak 2
		91.1 ± 1.4	average atmosphere	Leak 1, 2
		92.0 ± 0.5	surface only	Leak 2
D/H	HD, H_2	$(1.38 \pm 0.36) \times 10^{-4}$	120 to 62 km	Leak 1
		$(1.32 \pm 0.30) \times 10^{-4}$	21 km to surface	Leak 2
		$(1.35 \pm 0.30) \times 10^{-4}$	average atmosphere	Leak 1, 2
^{20}Ne mole fraction		$<2 \times 10^{-5}$	upper limit (noble gas cell)	Leak 3
$^{22}Ne/(N_2 + CH_4)$ tentative		$(2.8 \pm 2.1) \times 10^{-7}$	75–77 km (noble gas cell)	Leak 3
$^{36}Ar/(N_2 + CH_4)$		$(2.06 \pm 0.84) \times 10^{-7}$	75–77 km (noble gas cell)	Leak 3
^{38}Ar mole fraction		$<5 \times 10^{-8}$	upper limit (noble gas cell)	Leak 3
$^{40}Ar/(N_2 + CH_4)$		$(3.39 \pm 0.12) \times 10^{-5}$	75–77 km (noble gas cell)	Leak 3
$^{40}Ar/(N_2 + CH_4)$		$(3.35 \pm 0.25) \times 10^{-5}$	18 km to surface	Leak 2
Kr, Xe mole fraction		$<1 \times 10^{-8}$	upper limit (noble gas cell)	Leak 3

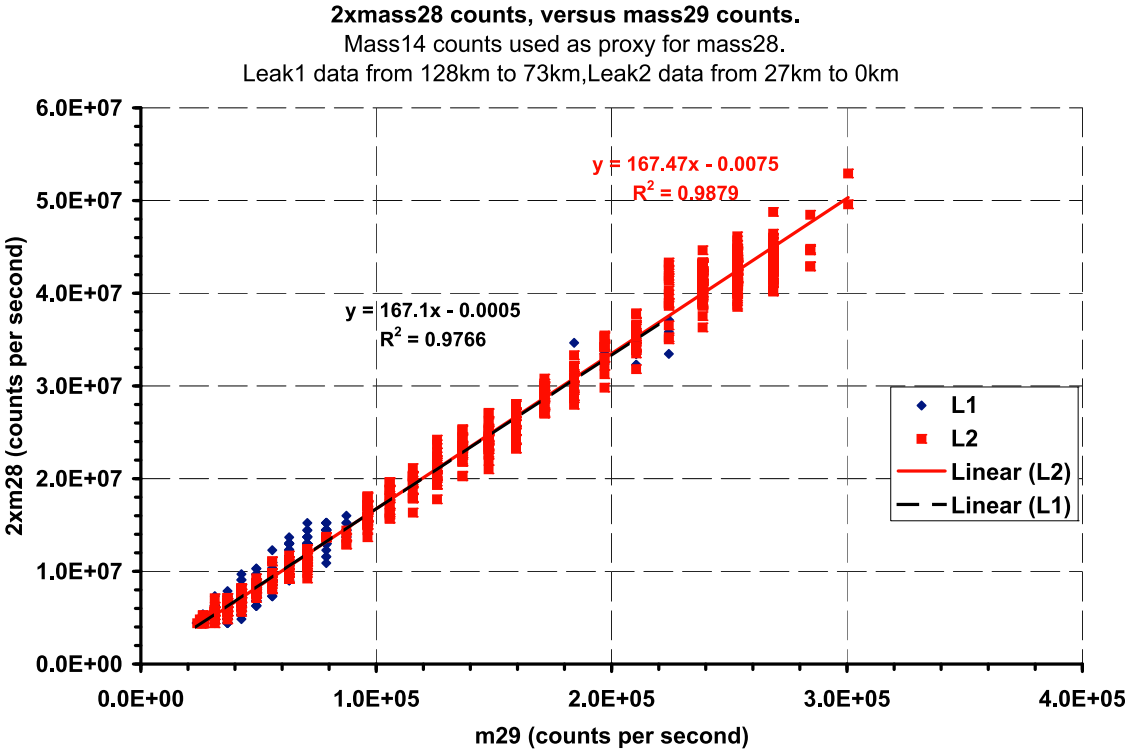

Figure 14. $m/z = 28$ counts multiplied by two ($m/z = 14$ is used as proxy) versus $m/z = 29$ counts. Leak L1 counts are dark blue diamonds, and leak L2 counts are red squares. The straight lines are least squares fits. The $m/z = 29$ counts were multiplied by molecular mass ratio $(28/29)^{1/2}$ to account for the gas flow difference in free molecular flow to the pumps.

spectrometers and results from slow outgassing from microscopic surface cracks and trapping volumes in the evacuated regions of the instrument. Prolonged bake out periods, on a high vacuum pumping speed processing system prior to launch, reduce it and other background gases but never do completely eliminate them in the time available for processing.

[60] Radiogenic ^{40}Ar was detected in the noble gas cell and directly during the descent. The average mole fraction from 18 km altitude to the surface is

$$^{40}Ar/(N_2 + CH_4) = (3.35 \pm 0.25) \times 10^{-5}. \quad (9)$$

Above 18 km altitude the direct measurement was obscured by the ^{40}Ar instrument background. The mole fraction computed from the noble gas cell measurement is

$$^{40}Ar/(N_2 + CH_4) = (3.39 \pm 0.12) \times 10^{-5}. \quad (10)$$

The mole fractions were computed from the $m/z = 40$ mass peak intensities. Laboratory calibration data and corrections were applied for dead time and contributions from a permanent ^{40}Ar instrument background. Contributions of hydrocarbons in the same mass range, for example, C_3H_4 are negligible based on heights of the fractionation peaks.

[61] Kr and Xe concentration levels were below the detection threshold of the instrument as can also be seen from the mass spectrum shown in Figure 12. The upper limit is at a mole fraction of 1×10^{-8}.

3.6. Isotope Ratios for the Major Gas Constituents

3.6.1. $^{14}N/^{15}N$ in Molecular Nitrogen

[62] The isotopic ratio of nitrogen was derived from the pulse count ratio at $m/z = 29$, $^{14}N^{15}N$, and $m/z = 28$, $^{14}N_2$. The count ratios plotted versus time from entry are shown in Figure 13, which also shows the count ratios plotted with $m/z = 14$, $^{14}N^+$, used as proxy for $^{14}N_2$. The regions where leak L1and leak L2 were used are shown in different colors as indicated in the legend. At times later than 1500 s for leak L1 and later than 7000 s for leak L2 the $m/z = 28$ counts are no longer valid due to counter saturation as can be seen by the slope changes. The species and molecular weight-dependent gas transmission through the capillary leaks was verified to be negligible for the difference of one mass unit and the differential count resolution of the instrument. Corrections were applied for the molecular weight depending on pumping speed of the vacuum pumps.

[63] The results are listed in Table 3 from regions where the statistical fluctuations were low and dead time corrections for the $m/z = 28$ peaks were also small. The average is

$$^{14}N/^{15}N = 167.7 \pm 0.6. \quad (11)$$

As mentioned above, the range of usable data points during the descent was extended by using dissociative ionized nitrogen $^{14}N^+$ at $m/z = 14$ as proxy for $^{14}N_2$. The contributions from dissociative ionization of methane, CH_2^+ at $m/z = 14$ were subtracted. The dissociation fractions were determined from flight data to be 0.0467 for N_2 and from the

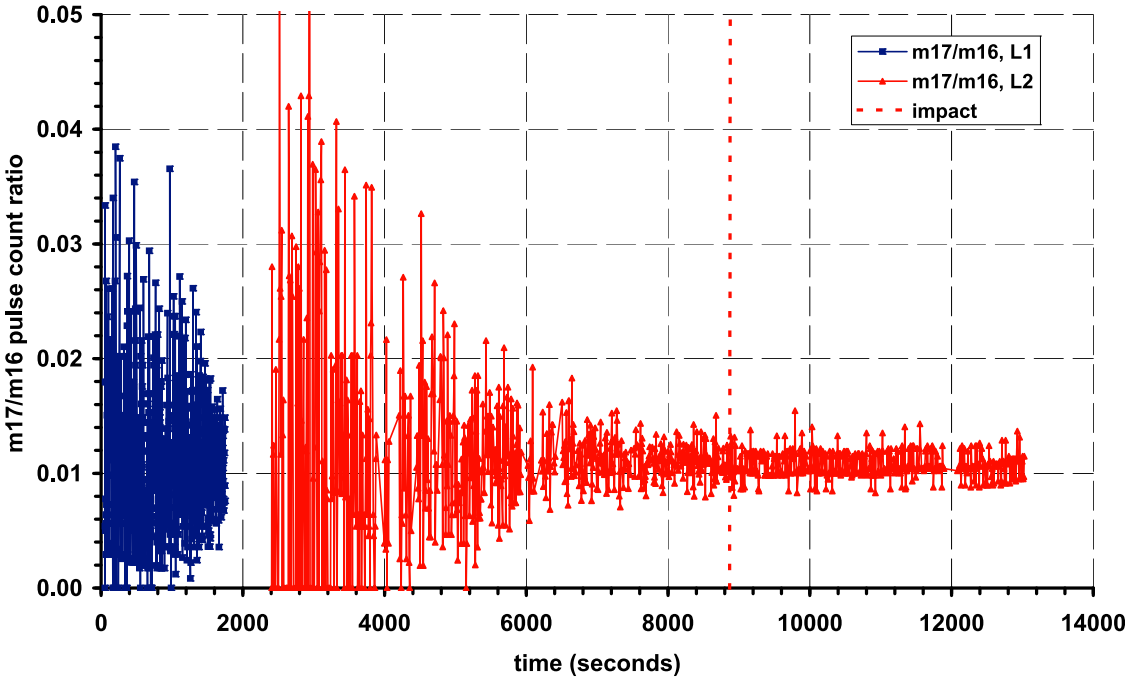

Figure 15. Pulse count ratios of all sample points of $m/z = 17$ to $m/z = 16$ due to CH_4, versus time from sequence initiation. Dark blue is from the leak L1 region, and red is from the leak L2 region. Surface impact is indicated by the vertical dashed red line.

noble gas cell data to be 0.0506 for CH_4. The result is shown in Figure 14 where the appropriately scaled pulse counts are plotted and the slope of the least squares fit is the isotope ratio $^{14}N/^{15}N$ after multiplication by the pumping speed ratio of $(29/28)^{0.5}$. The results are 167.1 ± 3.9 for the leak L1 and 167.5 ± 2 for the leak L2 region. These numbers are not listed in Table 3 and are presented only to show consistency of the data.

3.6.2. $^{12}C/^{13}C$ in Methane

[64] The carbon isotopic ratio was determined from methane, the major carbon-carrying molecule in the atmosphere of Titan. Data were analyzed from all regions of the atmosphere, the noble gas cell, and the surface. As mentioned above, methane is retained in the noble gas cell, and it serves as reference gas to determine noble gas mixing ratios. Pulse count ratios of $m/z = 17$ to $m/z = 16$ are plotted versus time from descent initiation in Figure 15, for the upper atmosphere region sampled through leak L1, and the lower atmosphere region and surface through leak L2. Methane ($^{12}CH_4$) is assumed to be the only significant contributor to the $m/z = 16$ counts. Contributions of fractionations from higher molecular weight species at $m/z = 16$ are negligible because of the high abundance of methane. The counts at $m/z = 17$ are the sum of counts from $^{13}CH_4$ and $^{12}CH_3D$. Both compounds cannot be separated by the mass spectrometer but the $^{12}CH_3D$ contribution can be obtained from the results for the $^{12}CH_3D/^{12}CH_4$ ratio of the CIRS experiment on the Cassini orbiter. A D/H ratio of 1.32×10^{-4} [*Bezard et al.*, 2007] was used to compute the $^{12}CH_3D$ contribution to the $m/z = 17$ counts. Fractionations from high molecular weight constituents do not add noticeably to the $m/z = 17$ count because none were seen by the mass spectrometer in high enough concentrations to matter. Ammonia, NH_3, either from the atmosphere or as chemical background is not expected to contribute to the $m/z = 17$ peak because its atmospheric mixing ratio would be too low and the detection would further be impeded by surface absorption in the instrument. A permanent ammonia background in the ion source has never been observed. The regions from which the isotopic ratios were computed are from 127 to 67 km altitude for leak L1, from a grab sample taken at 76.5 km for leak L3 (noble gas cell), and from 23 km to the surface and on the surface for leak L2. The values are listed in Table 3.

[65] The average atmospheric value is $^{12}CH_4/^{13}CH_4$ = 91.1 ± 1.4, the noble gas cell value is 91.7 ± 1.5, and the value for methane evaporated from the surface is 92.0 ± 0.5.

[66] These values are approximately 10% greater than the earlier preliminary results [*Niemann et al.*, 2005].

3.6.3. Deuterium in Molecular Hydrogen

[67] The D/H ratio in hydrogen in the atmosphere was determined from molecular hydrogen H_2 and deuterated hydrogen HD. The D/H isotope ratio is numerically very low since the H_2 abundance in the atmosphere is also small. The low pulse count rate at $m/z = 3$ (DH) reduces the time during the descent when the $m/z = 3$ pulse counts were sufficiently above the detection threshold to yield a valid measurement. The leak L1 region was generally preferred because it was free from possible interference from the molecular hydrogen that was used as a carrier gas later for the gas chromatograph subsystem. It was determined, however, that the carrier gas interference was small and could be subtracted. The data were averaged for all of the leak L1 regions and all of the leak L2 regions. Corrections were made for instrument carried hydrogen background, not associated with the H_2 carrier gas for the GC, and con-

tributions of dissociative ionized H_2^+ and HD^+ from methane. The methane contributions were determined from postflight laboratory calibration of the flight spare GCMS instrument. The D/H ratios are listed in Table 3.

[68] Although it is of interest to see a height profile of the D/H ratio, the count rates at $m/z = 3$ were too low to derive a meaningful profile.

3.7. Oxygen

[69] Oxygen-bearing constituents, e.g., H_2O and CO_2, were not in sufficient abundance in the atmosphere for an oxygen concentration and oxygen isotopic ratio measurement. CO could not be separated from N_2, as discussed previously. However, as is shown in Figure 9 and discussed in section 3.3, CO_2 was observed on the surface.

4. Discussion

[70] Preliminary results from the GCMS have been reported previously [*Niemann et al.*, 2005]. All the preliminary results provided in that report have changed to various degrees and are now superseded by the data provided in this paper. Calibration data applied from a thorough calibration of the flight spare instrument, a more accurate accounting of mass peak sizes (e.g., species interference) and dead time corrections of the pulse counting system and a more thorough examination and better use of the complete data set led to the results reported here.

[71] Molecular nitrogen is the most abundant gas in the atmosphere of Titan followed by a few percentage in mole fraction of methane. The total pressure on the surface is 1500 hPa. This was determined by many experiments using various techniques and refinements of the measurements.

[72] The GCMS results contributed a detailed altitude profile of the CH_4 and H_2 mole fractions in the lower atmosphere, the isotope ratios of $^{14}N/^{15}N$ in molecular nitrogen, $^{12}C/^{13}C$ in methane, and D/H in molecular hydrogen.

4.1. Methane (CH_4)

[73] The current CH_4 mole fraction of 5.5×10^{-2} just above the surface is subsaturated at a relative humidity of approximately 50%. While the mixing ratio of CH_4 remains nearly uniform with altitude up to approximately 7 km, its saturation vapor mixing ratio decreases rapidly with decreasing temperature above the surface (saturation vapor pressure of CH_4 above a mixture of N_2 dissolved in liquid CH_4 was based on *Kouvaris and Flasar* [1991]). Consequently, CH_4 reaches its lifting condensation level or 100% relative humidity at an altitude of approximately 7 km. This represents the base of condensation of CH_4 as liquid. The GCMS CH_4 data are consistent with saturation above liquid CH_4 with N_2 dissolved in it up to about 13–14 km. Above this altitude, a phase change to solid particles is expected, with the possible presence of supercooled droplets of a two component (methane-nitrogen) liquid as well. The nearly constant CH_4 mole fraction of 1.48×10^{-2} at the tropopause and above in the stratosphere is consistent with saturation above CH_4 ice and with the departure of the measured CH_4 mole fraction from the predicted *Kouvaris and Flasar* [1991] saturation values above approximately 14 km, as discussed previously by *Atreya et al.* [2006], and confirmed recently by laboratory simulation experiments [*Wang et al.*, 2009].

[74] The GCMS value is in agreement with the CIRS measurement of methane in the stratosphere [*Flasar et al.*, 2005]. Only at very high altitudes of ~600 km and higher-dose photochemistry begin to erode methane, thus depleting its mole fraction [*Wilson and Atreya*, 2004].

4.2. Molecular Hydrogen (H_2)

[75] The H_2 mole fraction determined from the GCMS data is in good agreement with previous determinations of the H_2 mole fraction in Titan by Voyager IRIS and Cassini CIRS experiments. The Voyager determination by *Courtin et al.* [2005] from $S_0(0)$ and $S_0(1)$ transitions of the H_2-N_2 dimers indicated a mole fraction of $(1.0 \pm 0.4) \times 10^{-3}$.

[76] The CIRS-Cassini determination is equal to $(9.6 \pm 2.4) \times 10^{-4}$ [*Courtin et al.*, 2007].

[77] Since Titan's atmosphere is mainly composed of N_2 and CH_4, substantial amounts of atomic hydrogen are produced by photochemical reactions during the formation of organic products. Theoretical models predict that atomic hydrogen recombines to form H_2 molecules [*Yung et al.*, 1984; *Wilson and Atreya*, 2004; *Strobel et al.*, 2009; *Cui et al.*, 2008; *Strobel*, 2009]. The models predict a constant volume mixing ratio of H_2 in the homosphere, consistent with the 1 Myr photochemical lifetime of H_2.

[78] In laboratory measurements, *Sekine et al.* [2008a] investigated heterogeneous reactions of atomic hydrogen with synthetic Titan tholins. Results suggested to the authors that these reactions might remove atomic hydrogen in the stratosphere and mesosphere of Titan. In a subsequent work, *Sekine et al.* [2008b] proposed a model of the total H_2 production and loss rate in the stratosphere, with an H loss peaking around 500 km altitude. As a consequence, the H_2 mixing ratio might not be constant with height. Thus, it may be premature to conclude that the INMS measurements of H_2 made at altitudes above 900 km [*Waite et al.*, 2005; *Yelle et al.*, 2006, 2008; *Cui et al.*, 2008] can be extrapolated monotonically to those measured in the lower atmosphere in situ by the Huygens GCMS and remotely by CIRS from the Cassini orbiter.

4.3. Carbon Dioxide (CO_2)

[79] Carbon dioxide was first detected in the atmosphere of Titan by the Voyager Infrared Radiometer Spectrometer at 667 cm^{-1} in the ν 2 band of the Q branch [*Samuelson et al.*, 1983]. These observations yielded an average mole fraction of 1.5 (+1.5, −0.8) ppbv above 110 hPa, later revised to approximately 14 ppbv between 100 and 200 km altitude following further analysis of the same data [*Coustenis et al.*, 1991]. This revision agrees with the Cassini CIRS results at the peak of the contribution function at 6.2 hPa [*Coustenis et al.*, 2007]. The CIRS data showed little change in CO_2 with latitude. While CO_2 remains subsaturated down to low stratospheric altitudes [*Baines et al.*, 2006], it is expected to condense at the tropopause where the temperature is 74 K, provided that some unknown process does not deplete it in the lower stratosphere. Some reevaporation of dry ice particles is expected during sedimentation below the tropopause down to the 94 K surface of Titan, but some CO_2 could be expected to survive in condensed form at the surface. The presence of solid CO_2 in the

surface of Titan was reported from an analysis of the Cassini visible and infrared mapping spectrometer [*McCord et al.*, 2008].

[80] The GCMS detected CO_2 on the surface of Titan as described in section 3.3.

[81] This CO_2 could have originated from one or more of the following sources: A reaction in the atmosphere between CO and externally delivered water vapor by way of CO + $OHCO_2$ + H [*Samuelson et al.*, 1983] where OH is derived from water vapor detected in Titan's upper atmosphere by ISO [*Feuchtgruber et al.*, 1999], or it could have been trapped as condensate on planetesimals that made Titan [e.g., *Hersant et al.*, 2008], or left over and outgasssed from the interior if methane was produced in Titan's interior [*Atreya et al.*, 2006].

[82] CO is uniformly mixed in Titan's atmosphere and believed to be primordial and outgassed from the interior in cryovolcanic events [*Baines et al.*, 2006]. A detailed height profile for CO_2 is not yet available. The measured CO/CO_2 ratio in Titan's stratosphere is approximately 2300, with CO at 33 ppm based on the Cassini visual and infrared mapping spectrometer (VIMS) measurements [*Baines et al.*, 2006; *Bellucci et al.*, 2009] and 32 ppm from ground-based measurements [*Lellouch et al.*, 2004]. This is nearly a factor of 2000 greater than the value of 1.3 estimated for comets [*Boice and Huebner*, 1997].

[83] Any outgassing of CO_2 (and CO) from the interior might be expected to be associated with traces of other volatiles, especially H_2O, NH_3, and H_2S. The GCMS surface data do not show evidence of these gases. This does not imply that they are not present on the surface. The GCMS only samples the warmed area of Titan's surface in the immediate vicinity of the inlet. The H_2O saturation vapor pressure at the suspected evaporation temperature of 145 K [*Lorenz et al.*, 2006] is only 1.3×10^{-8} hPa or a mole fraction of 8.7×10^{-12} relative to the 1500 hPa atmospheric pressure at the surface. This is well below the normal GCMS detection capability. The NH_3 vapor pressure is 67.7 hPa or a mole fraction of 4.5×10^{-5}, which is within the detection range of the GCMS. However, the $m/z = 17$ peak is masked by much higher contributions from $^{13}CH_4$ and $^{12}CH_3D$ that made the detection impossible. Although a saturated mole fraction of H_2S (2×10^{-3}) would be detectable by the GCMS, the measured H_2S at $m/z = 34$ was below the detection threshold of the GCMS in this mass range. The GCMS derived upper limit is 5×10^{-8}. The threshold is raised above 1×10^{-8} because of background counts occurring at high ion source pressures.

4.4. Protosolar Noble Gases

[84] The Huygens GCMS spectra clearly show the presence of the protosolar isotope of argon, ^{36}Ar, with a mixing ratio of $(2.1 \pm 0.8) \times 10^{-7}$. There are no indications of Kr and Xe with their upper limits being 10 ppb [*Niemann et al.*, 2005; this work]. This led several investigators to suggest models for the evolution of the atmosphere that would account for the absence of these two gases. These models included formation of clathrates on the surface of Titan [*Thomas et al.*, 2007; *Osegovich and Max*, 2005] or formation and sequestration of clathrates in a putative subsurface ocean [*Tobie et al.*, 2006] or capture by aerosols with subsequent precipitation [*Jacovi and Bar-Nun*, 2008].

[85] However, *Owen and Niemann* [2009] demonstrated that the relative abundances of noble gases in known reservoirs in the solar system, the Sun, Venus, Earth, Mars and meteorites, would allow the Huygens GCMS to detect ^{36}Ar, but not the other two gases. The instrument simply did not have the sensitivity to detect Kr and Xe given the observed abundance of ^{36}Ar in any of these reservoirs. Although the processes proposed for the nondetection of krypton and xenon may be operating on Titan, the available data do not reveal or require them [*Owen and Niemann*, 2009]. Of course, Titan might have collected its noble gases from a completely different mixture from those we know. The only constraint we can offer on such unknown mixtures is that the depletion of argon relative to krypton could not be greater than it is on Mars or the Earth.

[86] The origin of argon on Titan can be explored by comparing the solar value of $^{14}N/^{36}Ar$ with the values in the atmospheres of Titan, Mars, and Earth, once they have been reconstructed for escape [*Lunine et al.*, 1999]. The solar value of $^{14}N/^{36}Ar$ is 30 [*Grevesse et al.*, 2007]. On Earth and Mars, it is $\sim 4 \times 10^4$ while on Titan, it is $\sim 1 \times 10^7$.

[87] There are several ways of explaining these differences but a detailed treatment of appropriate models is beyond the scope of this paper.

[88] The discovery of ^{22}Ne provides yet another perspective. On Titan, $^{22}Ne/^{36}Ar \sim 1$, but with the caveat that the ^{22}Ne is tentative and has a large uncertainty (section 3.5). On the Sun, it is 3; on Earth and Venus, it is 0.04; in the C3V meteorite Allende, the ratio is 0.02. It is virtually impossible to trap Ne in ice except in amorphous ice at ambient temperatures of about 20–25 K [*Laufer et al.*, 1987]. There are not yet any detections of Ne or any other noble gases in comets [*Weaver et al.*, 2002]. The implications of the detection of neon in Titan's atmosphere require further investigation.

[89] The cold outer solar nebula should duplicate chemical conditions in the interstellar cloud from which it formed. The basic features of these conditions should be captured in comets. Yet comets do not reveal either the abundances or molecular species in the interstellar medium as expected. In the ISM, N_2 is typically 10 times more abundant than NH_3, whereas in the comae of comets, NH_3 is the dominant carrier of N. There is only an upper limit on N_2 that is in orders of magnitude below the expected abundance. Argon was not detected either, with an upper limit of about 10% of the solar value for Ar/O [*Weaver et al.*, 2002]. The presence of NH_3 and the strong depletion of N_2 are clear and striking [*Cochran et al.*, 2000; *Bockelee-Morvan et al.*, 2004]. This suggests that an efficient process precluded the trapping of detectable (so far!) amounts of N_2 and Ar in cometesimals.

[90] However, ^{36}Ar was clearly measured in Titan's atmosphere by the Huygens GCMS, and N_2 has been known to be the major atmospheric constituent since Voyager discovered it. The tiny amount of ^{36}Ar must be primordial, but N_2 is currently assumed to be the product of NH_3 photodissociation in the warm early atmosphere of Titan [*Atreya et al.*, 2009]. There are several possible processes that could lead to the value of $^{36}Ar/^{14}N$ that is observed in Titan's atmosphere today, both in the capture of these gases from the solar nebula and in their pre-appearance histories on Titan [*Bar-Nun et al.*, 1988; *Huebner and McKay*, 1991; *Iro et al.*, 2003; *Hersant et al.*, 2008]. The discovery of ^{36}Ar

therefore provides a new basis for future studies of Titan. The acquisition of new noble gas data from Titan must wait a decade or more. Meanwhile our best hope for some enlightenment is perhaps the measurement of noble gases and nitrogen from Comet Churyumov-Gerasimenko by the Rosetta mission.

4.5. Radiogenic Argon

[91] Radiogenic ^{40}Ar is a decay product of potassium 40 (^{40}K), which has a half-life of 1.28 billion years. Thus, over the age of the solar system most of the radiogenic argon on Titan has been produced and its abundance in the atmosphere is potentially an indicator of the extent to which outgassing of volatile elements has occurred from the deep interior, where the rock (hence the potassium) should reside. If the rocky component of the interior of Titan has the same composition as that of the Earth and has outgassed to the same extent, ^{40}Ar should be much more abundant than measured, comprising ~0.05% of the atmosphere [*Owen*, 1982] (corrected for loss of N). Evidently the outgassing or cycling of volatiles to the surface was not as much as on the Earth. Nevertheless the presence of the ^{40}Ar at the levels seen in Titan's atmosphere is a strong indication that Saturn's largest moon has had a geologically active past and is consistent with the view that methane has been outgassed from Titan's interior over geologic time, replacing that depleted in the atmosphere by chemistry energized by ultraviolet photons and by charged particles.

4.6. Nitrogen ^{14}N/^{15}N Isotope Ratio

[92] The revised GCMS result confirms that the ^{14}N/^{15}N ratio of 167.7 in N_2 on Titan today is substantially different from the telluric value of 272 [*Anders and Grevesse*, 1989]. This is additional information to help understand the isotope ratios measured in the solar system that suggests large scale isotope heterogeneity in the early solar nebula [*Marty et al.*, 2010]. Using data from the Cassini ion and neutral mass spectrometer (INMS) *Mandt et al.* [2009] arrive at a value of ^{14}N/^{15}N = 143 for the lower, mixed atmosphere. The discrepancy between the GCMS and the INMS could be the result of model-dependent extrapolation of the INMS data from the region of measurements above 1000 km to the homosphere.

[93] It is difficult to determine the value of ^{14}N/^{15}N in the primitive atmosphere of Titan.

[94] There is a large consensus for the hypothesis that NH_3 not N_2 was the dominant form of nitrogen in the solar nebula and in the Saturn subnebula where Titan was formed [*Atreya et al.*, 2009]. The nitrogen isotope ratios in NH_3 in comets and representative protosolar bodies, which contributed nitrogen to the atmosphere, e.g., in icy grains have not yet been measured so that we do not know the value in NH_3 on early Titan.

[95] Several scenarios for interpreting the ^{14}N/^{15}N ratio measured on Titan today can be envisaged. The first scenario was to assume that a very large nitrogen escape occurred during the evolution of Titan [*Lunine et al.*, 1999; *Lammer et al.*, 2000]. This permits us to assume a large initial isotopic ratio, even the telluric ratio of 272 [*Anders and Grevesse*, 1989]. However, *Mandt et al.* [2009] have calculated that, considering the large amount of N_2 that must be fractionated, the initial ^{14}N/^{15}N cannot have changed much due to atmospheric processes and the initial isotopic ratio should have been close to 167. A detailed treatment of the subject is given by *Atreya et al.* [2009].

4.7. Carbon ^{12}C/^{13}C Isotope Ratio

[96] The value of ^{12}C/^{13}C determined in the local interstellar medium is 43 ± 4 [*Hawkins and Jura*, 1987]. In evaluating this determination, it is important to remember that the Sun has revolved around the center of the galaxy 15–20 times since the origin of the solar system. Thus the "local" Interstellar Medium today is not the one in which the solar system formed. Furthermore, galactic evolution will lower the ratio with time. There is, however, a remarkable uniformity of ^{12}C/^{13}C = 90 ± 5 in every solar system object that has been measured with sufficient precision (Table 4). Accordingly, we adopt the solar value of 90 as our standard reference [*Anders and Grevesse*, 1989]. This choice is strongly supported by the most recent observations of the coma of comets. *Manfroid et al.* [2009] give 91.0 ± 3.6 for the ratio in 23 comets of various dynamical classes. We therefore expect to find a value of ^{12}C/^{13}C close to 90 in Titan's hydrocarbons. Indeed the GCMS found ^{12}C/^{13}C = 91.4 ± 1.5 for methane in Titan's atmosphere and 92.0 ± 0.5 at the surface (Niemann et al., this work).

[97] These values can be compared with measurements made by remote sensing.

[98] Analyses of 15 IR spectra covering bands of CH_4, C_2H_2, and C_2H_6 with the Cassini orbiter Composite Infrared Spectrometer (CIRS) by *Nixon et al.* [2008a] produced an average value of ^{12}C/^{13}C = 80.8 ± 2. Individual measurements were CH_4: 76.6 ± 2.7, C_2H_2: 84.8 ± 3.2, C_2H_6: 89.8 ± 7.3. *Nixon et al.* [2008b] found a value of 84 ± 17 for this ratio in CO_2. *Jennings et al.* [2009] reported ^{12}C/^{13}C = 89 ± 8 from ground-based observations of C_2H_6. It is too soon to attempt an analysis of the reason(s) for the disagreement among these different measurements.

[99] The preliminary reported value of ^{12}C/^{13}C in methane derived from GCMS data was 82.3 ± 1 [*Niemann et al.*, 2005]. This value is noticeably lower than the terrestrial value of the reference inorganic standard value of 89.4 (NIST or Vienna-Pee Dee Belemnite, V-PDB). Since terrestrial carbon-based biological activity is usually associated with an isotopic fractionation that favors light carbon [*Farquhar et al.*, 1989], we suggested that this preliminary value of ^{12}C/^{13}C did not support a possible biological origin for CH_4. It is now clear that the stand alone ratio ^{12}C/^{13}C = 91.4 ± 1.5 (Niemann et al., this work) in Titan's methane does not allow any conclusions to be drawn on the existence of biological activity on Titan past or present.

4.8. Deuterium-Hydrogen Isotope Ratio

[100] The D/H ratio in hydrogen obtained by the GCMS is $(1.35 \pm 0.3) \times 10^{-4}$. As outlined in section 3.6, the D/H ratio is determined from the measurement of the ratio of HD to H_2 present in the atmosphere of Titan. These gases are presumably products of photolysis of CH_4. Therefore, it may not be too surprising that the ratio derived from GCMS measurements agrees with the value of $1.32(+0.15/-0.11) \times 10^{-4}$ derived from CH_3D/CH_4 measured by the CIRS instrument in the stratosphere of Titan [*Bezard et al.*, 2007].

[101] The low enhancement of this Titan D/H ratio for hydrogen relative to the protosolar D/H ratio in hydrogen of

Table 4. $^{12}C/^{13}C$ in the Solar System

1. Standards		
Earth	90.0	NIST (V-PDB)
Meteorites (Sun)	90.0	*Anders and Grevesse* [1989]
2. Solar system		
Venus	90 ± 3	*von Zahn et al.* [1983]
Mars	90 ± 5	*Owen* [1992]
Jupiter	$92.5^{+4.5}_{-4.0}$	*Niemann et al.* [1998]
Saturn	$91.8^{+8.4}_{-7.8}$	*Fletcher et al.* [2009]
23 Comets	91.0 ± 3.6	*Manfroid et al.* [2009]
Summary – solar system		
Inner	90	
Outer	92	
3. Titan		
Molecule	Result	INST
(A) Remote sensing		
CH_4	76.6 ± 2.7	CIRS *Nixon et al.* [2008a]
C_2H_2	84.8 ± 3.2	CIRS *Nixon et al.* [2008a]
C_2H_6	89.8 ± 7.3	CIRS *Nixon et al.* [2008a]
C_2H_6	89.0 ± 8	CIRS *Jennings et al.* [2009]
CO_2	84 ± 17	CIRS *Nixon et al.* [2008b]
(B) In situ		
CH_4	91.1 ± 1.4 (atm.) 92.0 ± 0.5 (surface)	GCMS Niemann et al. (this work)

$(2.1 \pm 0.5) \times 10^{-5}$ [*Geiss and Gloecker*, 1998] or $(2.6 \pm 0.7) \times 10^{-5}$ [*Mahaffy et al.*, 1998] is, however, difficult to interpret. The Titan D/H ratio is lower than the D/H ratios in cometary water, which varies from 2.9×10^{-4} to 4.1×10^{-4} as measured in four comets [*Villanueva et al.*, 2009], and in the water plumes escaping from Enceladus, as measured by the INMS experiment, which is $2.9(+1.5/-0.7) \times 10^{-4}$ [*Waite et al.*, 2009]. A more efficient deuterium exchange between water and protosolar hydrogen relative to methane with H_2 is unattractive because laboratory measurements have provided evidence that in a neutral environment the isotopic exchange is weaker than that of water with hydrogen [*Lecluse and Robert*, 1994].

[102] The D/H ratio in cometary methane might be smaller than the D/H ratio in cometary water [*Mousis et al.*, 2002] implying a similar behavior in the protosolar cloud. According to available isotope chemistry models, this seems unlikely. Our best chance to improve the situation would be to determine the D/H ratio in methane in a comet from ground-based observations or from the Rosetta mission. Equally of value would be to measure the D/H ratio in water ice at the surface of Titan [*Coustenis et al.*, 2009].

4.9. Organic Species Evaporating From the Surface

[103] The different volatilities of each component either in pure form or in mixtures with other species including nitrogen and the large uncertainty about the surface contact parameters make it difficult to relate the observations quantitatively to surface concentrations. It is noticeable though that those molecules, which would be on the surface at the landing site in liquid form as possibly droplets, reach a constant partial pressure. CH_4 and C_2H_6 fall into that group. The others, which would be sublimating from solids (ices), never reached a constant level through the end of the GCMS surface measurements. This indicates that the temperature environment in the sampling area on the surface was transient for the duration. A reservoir of the evaporating liquids must have been able to hold enough liquids to last for the duration of the surface sampling. Flash evaporation from thin layer condensation on stable aerosols is less likely because the rate would vary more with time. It is thus likely that there was a reservoir of condensed species on the surface at the Huygens landing site.

[104] **Acknowledgments.** We acknowledge the Huygens Atmospheric Structure Instrument (HASI) team for providing the atmospheric pressure-temperature-altitude data to the GCMS team. We thank D. Strobel for his discussion on atmospheric loss and for providing a preprint of his paper on molecular hydrogen in Titan's atmosphere. The contributions of personnel at NASA Goddard Space Flight Center (GSFC), University of Michigan, University of Paris, and Ohio State University are acknowledged. We are indebted to Eric Raaen of GSFC for his continued support in instrument testing, data analysis, and development of laboratory software. We thank Kiran Patel of GSFC for the assistance he provided for the postlaunch instrument calibration. We also thank the personnel at the European Space Research and Technology Centre (ESTEC) and the European Space Operations Center (ESOC) for their technical support and guidance during this mission. We acknowledge NASA, ESA, and CNES for support of the mission.

References

Anders, E., and N. Grevesse (1989), Abundances of the elements: Meteoritic and solar, *Geochim. Cosmochim. Acta.*, *53*, 197–214.

Atreya, S. K., et al. (2006), Titan's methane cycle, *Planet Space Sci.*, *54*, 1177–1187.

Atreya, S. K., et al. (2009),Volatile origin and cycles: Nitrogen and methane, in *Titan From Cassini-Huygens*, edited by R. H. Brown et al., chap. 7, pp. 177–199, Springer, Heidelberg.

Baines, K. H., et al. (2006), On the discovery of CO nighttime emissions on Titan by Cassini/VIMS: Derived stratospheric abundances and geological implications, *Planet Space Sci.*, *54*, 1552–1562.

Bar-Nun, A., et al. (1988), Trapping of gas mixtures by amorphous water ice, *Phys. Rev. B*, *38*, 7749.

Bellucci, A., et al. (2009), Titan solar occultation observed by Cassini/VIMS: Gas absorption and constraint on aerosol composition, *Icarus*, *201*, 198–216.

Bezard, B., et al. (2007), Detection of $^{13}CH_3D$ on Titan, *Icarus*, *191*, 397–400.

Biemann, K. (2006), Astrochemistry: Complex organic matter in Titan's aerosols?, *Nature*, *444*, E6, doi:10.1038/nature05417.

Bockelee-Morvan, D., et al. (2004), The composition of cometary volatiles, in *Comets II*, edited by M. Festou, H. U. Keller, and H. A. Weaver, pp. 391–425, Univ. of Arizona, Tucson.

Boice, D. C., and W. F. Huebner (1997), Comet: Structure and composition, in *Encyclopedia of Planetary Sciences*, edited by J. H. Sirley and R. W. Fairbridge, pp. 145–153, Chapman and Hall, London.

Broadfoot, A. L., et al. (1981), Extreme ultraviolet observations from Voyager 1 encounter with Saturn, *Science*, *212*, 206–211.

Cochran, A. L., et al. (2000), N_2^+ and CO^+ in Comets 122P/1991 S1 (deVico) and C/1995O1 (hale-Bopp), *Icarus*, *146*, 583–591.

Courtin, R., D. Gautier, and C. P. McKay (2005), Titan's thermal emission spectrum: Reanalysis of the Voyager infrared measurements, *Icarus*, *114*, 144–162.

Courtin, R., C. K. Sim, S. J. Kim, and D. Gautier (2007), The tropospheric abundance of Titan from the Cassini CIRS investigation, *Bull. Am. Astron. Soc.*, *39*, 529.

Coustenis, A., B. Bezard, and D. Gautier (1989), Titan's atmosphere from Voyager infrared observations: I. The gas composition of Titan's equatorial region, *Icarus*, *80*, 54–76.

Coustenis, A., et al. (1991), Titan's atmosphere from Voyager infrared observations: III. Vertical distribution of hydrocarbons and nitriles near Titan's north pole, *Icarus*, *89*, 152–167.

Coustenis, A., et al. (2007), The composition of Titan's stratosphere from Cassini/CIRS mid-infrared spectra, *Icarus*, *189*, 35–62, doi:10.1016/j.icarus.2006.12.022.

Coustenis, A., et al. (2009), TandEM: Titan and Enceladus mission, *Exp. Astron.*, doi:10.1007/s10686-008-9103-z.

Cui, J., R. V. Yelle, and K. Volk (2008), Distribution and escape of molecular hydrogen in Titan's thermosphere and exosphere, *J. Geophys. Res.*, *113*, E10004, doi:10.1029/2007JE003032.

Cui, J., et al. (2009), Analysis of Titan's neutral upper atmosphere from Cassini ion neutral mass spectrometer measurements, *Icarus*, *200*, 581–615.

Farquhar, G. D., J. R. Ehleringer, and K. T. Hubick (1989), Carbon isotope discrimination and photosynthesis, *Annu. Rev. Plant Physiol. Plant Mol. Biol.*, *40*, 503–537.

Feuchtgruber, H., et al. (1999), The universe as seen by ISO, in *ESA Publication Division, Noordwijk*, edited by P. Cox and M. F. Kessler, p. 133, ESA Publ. Div., Noordwijk.

Flasar, F. M., et al. (2005), Titan's atmospheric temperatures, winds, and composition, *Science*, *308*, 975–978.

Fletcher, L. N., et al. (2009), Methane and its isotopologues on Saturn from Cassini/CIRS observations, *Icarus*, *199*, 351–367.

Fulchignoni, M., et al. (2005), In situ measurements of the physical characteristics of Titan's environment, *Nature*, *438*, 785–791.

Geiss, J., and G. Gloecker (1998), Abundances of deuterium and helium 3 in the protosolar cloud, *Space Sci. Rev.*, *84*, 239–250.

Grevesse, N., M. Asplund, and A. J. Sauval (2007), The solar chemical composition, *Space Sci. Rev.*, *130*, 105–114.

Hanel, R., et al. (1981), Infrared observations of the Saturnian system from Voyager 1, *Science*, *212*, 192–200.

Hawkins, I., and M. Jura (1987), The $^{12}C/^{13}C$ isotope ratio of the interstellar medium in the neighborhood of the sun, *Astrophys. J.*, *317*, 926.

Hersant, F., et al. (2008) Interpretation of the carbon abundance in Saturn measured by Cassini, *Planet. Space Sci.*, *56*, 1103–1111.

Huebner, W. F., and C. McKay (1991), Chapter VIII, in *Physics and Chemistry of Comets*, edited by W. F. Huebner, 380 pp., Springer, Heidelberg.

Iro, N., et al. (2003), An interpretation of the nitrogen deficiency in comets, *Icarus*, *161*, 511–522.

Israel, G., et al. (2002), Huygens probe aerosol collector pyrolyser experiment, *Space Sci. Rev.*, *104*, 435–466.

Israël, G., et al. (2005), Complex organic matter in Titan's atmospheric aerosols from in situ pyrolysis and analysis, *Nature*, *438*, 796–799.

Israel, G., et al. (2006), Astrochemistry: Complex organic matter in Titan's aerosols? (Reply), *Nature*, *444*, E6, doi:10.038/nature05418.

Jacovi, R., and A. Bar-Nun (2008), Removal of Titan's noble gases by their trapping in its haze, *Icarus*, *196*, 302–304.

Jennings, D. E., et al. (2009), $^{12}C/^{13}C$ ratio N in ethane on Titan and implications for methane's replenshipment, *J. Phys. Chem. A.*, *113*, 11,101–11,106.

Kazeminejad, B., et al. (2007), Huygens' entry and descent through Titan's atmosphere—Methodology and results of the trajectory reconstruction, *Planet Space Sci.*, *55*, 1845–1876.

Kouvaris, L. C., and F. M. Flasar (1991), Phase equilibrium of methane and nitrogen at low temperatures—Application to Titan, *Icarus*, *91*, 112–124.

Kuiper, P. (1944), Titan: A satellite with an atmosphere, *Astrophys. J.*, *100*, 378–381.

Kunde, V. G., et al. (1981), C_4H_2, HC_3N and C_2N_2 in Titan's atmosphere, *Nature*, *292*, 686–688.

Lammer, H. W., et al. (2000), Nitrogen isotope fractionation and its consequence for Titan's atmospheric evolution, *Planet. Space Sci.*, *48*, 529–543.

Laufer, D., et al. (1987), Structure and dynamics of amorphous water ice, *Phys. Rev. B*, *36*, 9219–9227.

Lebreton, J.-P., et al. (2005), An overview of the descent and landing of the Huygens probe on Titan, *Nature*, *438*, 758–764, doi:101038/nature04347.

Lecluse, C., and F. Robert (1994), Hydrogen isotope exchange reaction rates: Origin of water in the inner solar system, *Geochim. Cosmochim. Acta*, *58*, 2927–2939.

Lellouch, E., et al. (2004), Titan's 5-micron lightcurve, *Icarus*, *168*, 209–214.

Lorenz, R. D., et al. (2006), Titan's damp ground: Constraints on Titan surface thermal properties from the temperature evolution of the Huygens GCMS inlet, *Meteor. Planet. Sci.*, *41*, 1705–1714.

Lunine, J. I., Y. L. Yung, and R. D. Lorenz (1999), On the volatile inventory of Titan from isotopic abundances in nitrogen and methane, *Planet. Space Sci.*, *47*, 1291–1303.

Magee, B. A., et al. (2009), INMS-derived composition of Titan's upper atmosphere: Analysis methods and model comparison, *Planet. Space Sci.*, *57*, 1895–1916.

Mahaffy, P. R., et al. (1998), Galileo probe measurement of D/H and 3He/4He in Jupiter's atmosphere, *Space Sci. Rev.*, *84*, 251–263.

Mandt, K. E., et al. (2009), Isotopic evolution of the major constituents of Titan's atmosphere based on Cassini data, *Planet. Space Sci.*, *57*, 1917–1930.

Manfroid, J., et al. (2009), The CN isotopic ratios in comets, *Astron. Astrophys.*, *503*, 613–624.

Marty, B., et al. (2010), Nitrogen isotopes in the récent solar wind from the analysis of Genesis targets: Evidence for large scale isotope heterogeneity in the early solar system, *Geochim. Cosmochim. Acta*, *74*, 310–355.

McCord, T. B., et al. (2008), Titan's surface: Search for spectral diversity and composition using the Cassini VIMS investigation, *Icarus*, *194*, 212–242.

Mousis, O., et al. (2002), The D/H ratio in methane in Titan. Origin and history, *Icarus*, *159*, 156–165.

Niemann, H., et al. (1998), The composition of the Jovian atmosphere as determined by the Galileo probe mass spectrometer, *J. Geophys. Res.*, *103*(E10), 22,831–22,845.

Niemann, H. B., et al. (2002), The gas chromatograph mass spectrometer for the Huygens probe, *Space Sci. Rev.*, *104*, 553–591.

Niemann, H. B., et al. (2005), The abundances of constituents of Titan's atmosphere from the GCMS instrument on the Huygens probe, *Nature*, *438*, 779–784.

Nixon, C. A., et al. (2008a), The $^{12}C/^{13}C$ isotopic ratio in Titan by hydrocarbons from Cassini/CIRS infrared spectra, *Icarus*, *195*, 778–791.

Nixon, C. A., et al. (2008b), Isotopic ratios in Titan's atmosphere from Cassini CIRS limb sounding: CO_2 in the equator and south, *Astrophys. J.*, *681*, L101–L103.

Osegovich, J. P., and M. D. Max (2005), Compound clathrate hydrate on Titan's surface, *J. Geophys. Res.*, *110*, E08005, doi:10.1029/2004JE002397.

Owen, T. (1992), *The Composition and Early History of the Atmosphere in Mars*, edited by H. H. Kiever et al., pp. 818–834, Univ. of Arizona, Tucson.

Owen, T., and H. B. Niemann (2009), The origin of Titan's atmosphere: Some recent advances, *Phil. Trans. R. Soc. A*, *367*, 607–615, doi:10.1098/rsta.2008.0247.

Owen, T. C. (1982), The composition and origin of Titan's atmosphere, *Planet. Space Sci.*, *30*, 833–838.

Samuelson, R. E., et al. (1983), CO2 on Titan, *J. Geophys. Res.*, *88*(A11), 8709–8715, doi:10.1029/JA088iA11p08709.

Sekine, Y., et al. (2008a), The role of organic haze in titan's atmospheric chemistry: I. Laboratory investigation on heterogeneous reaction of atomic hydrogen with Titan tholin, *Icarus*, *194*, 186–200.

Sekine, Y., et al. (2008b), The role of organic haze in Titan's atmospheric chemistry: II. Effect of heterogeneous reaction to the hydrogen budget and chemical composition of the atmosphere, *Icarus*, *194*, 201–211.

Shemansky, D. E., et al. (2005), The Cassini UVIS stellar probe of the Titan atmosphere, *Science*, *308*, 978–982.

Strobel, D. F. (2009), Titan's hydrodynamically escaping atmosphere, *Icarus*, *193*, 588–594.

Strobel, D. F., et al. (2009), Atmospheric structure and composition, in *Titan From Cassini-Huygens*, edited by R. H. Brown et al., chap. 10, pp. 235–257, Springer, Heidelberg.

Thomas, C., O. Mousis, V. Ballenegger, and S. Picaud (2007), Clathrate hydrates as a sink of noble gases in Titan's atmosphere, *Astron. Astrophys.*, *474*, L17-L20.

Tobie, G., J. I. Lunine, and C. Sotin (2006), Episodic outgassing as the origin of atmospheric methane on Titan, *Nature*, *440*, 61–64, doi:10.1038/nature04497.

Tyler, G. L., et al. (1981), Radio science investigations of the Saturn system with Voyager 1: Preliminary results, *Science*, *212*, 201–205.

Villanueva, G. L., et al. (2009), A sensitive search for deuterated water in Comet 8P/Tuttle, *Astrophys. J.*, *690*, L5–L9.

von Zahn, U., et al. (1983), *Composition of the Venus atmosphere in Venus*, edited by D. M. Hunter et al., pp. 299–430, Univ. of Arizona, Tucson.

Waite, J. H., Jr. et al. (2005), Ion neutral mass spectrometer results from the first flyby of Titan, *Science*, *308*, 982–986.

Waite, J. H., Jr. et al. (2007), The process of Tholin formation in Titan's upper atmosphere, *Science*, *316*, 870–875.

Waite, J. H., Jr. et al. (2009), Liquid water on Enceladus from observations of ammonia and ^{40}Ar in the plume, *Nature*, *460*, 487–490.

Wang, C. C., et al. (2009), Evidence for layered methane clouds in Titan's troposphere, *Icarus*, *206*, 787–790, doi:10.1016/j.icarus.2009.11.022.

Weaver, H. A., et al. (2002), A search for and O VI in three comets using the far ultraviolet spectroscopic explorer, *Astrophys. J.*, *576*, L95–L98.

Wilson, E. H., and S. K. Atreya (2004), Current state of modeling the photochemistry of Titan's mutually dependent atmosphere and ionosphere, *J. Geophys. Res.*, *109*, E06002, doi:10.1029/2003JE002181.

Yelle, R. V., et al. (2006), The vertical structure of Titan's upper atmosphere from Cassini ion neutral mass spectrometer measurements, *Icarus*, *182*, 567–576.

Yelle, R. V., et al. (2008), Eddy diffusion and methane escape from Titan's atmosphere, *J. Geophys. Res.*, *113*, E10003, doi:10.1029/2007JE003031.

Yung, Y. L., M. Allen, and J. P. Pluto (1984), Photochemistry of the atmosphere of Titan: Comparison between model and observations, *Astrophys. J.*, *55*, 465–506, doi:10.1086/190963.

S. K. Atreya, Department of Atmospheric, Oceanic and Space Sciences, University of Michigan, Ann Arbor, MI 48109-2143, USA.

J. E. Demick, Department of Physics and Physical Science, Huntington College, Bellingrath 307A, 1500 East Fairview Ave., Montgomery, AL 36106, USA.

D. Gautier, LESIA, Observatoire de Paris-Meudon, F-92195 Meudon Cedex, France.

J. A. Haberman, D. N. Harpold, W. T. Kasprzak, and H. B. Niemann, National Aeronautics and Space Administration, Mail Code 699, Greenbelt, MD 20771, USA. (hasso.b.niemann@nasa.gov)

J. I. Lunine, Department of Physics, University of Rome Tor Vergata, via della Ricerca Scientifica, I-00133 Rome, Italy.

T. C. Owen, Institute for Astronomy, University of Hawaii, Honolulu, HI 96822, USA.

F. Raulin, LISA, CNRS/Université Paris 12/Université Paris 7, Ave. General de Gaulle, F-94000 Creteil, France.